

**ASPECTS OF THE MCMASTER INTENSE POSITRON BEAM
FACILITY**

**ASPECTS OF THE MCMASTER INTENSE POSITRON BEAM
FACILITY (MIPBF)**

By PEIHAI LI

M.Eng., B.Sc.

A Thesis

Submitted to the School of Graduate Studies in Partial Fulfillment of the
Requirements for the Degree of Master of Applied Science

McMaster University © Copyright by Peihai Li, February 2015

McMaster University MASTER OF APPLIED SCIENCE (2015)
Hamilton, Ontario (Engineering Physics)

TITLE: Aspects of The McMaster Intense Positron Beam Facility
(MIPBF)

AUTHOR: Peihai Li, M.Eng. (Wuhan University)

SUPERVISOR: Professor Peter Mascher

NUMBER OF PAGES: xi, 113

Abstract

The McMaster Intense Positron Beam Facility (MIPBF) is a project based on the McMaster Nuclear Reactor (MNR) that aims to set up the first intense positron beam in Canada. The final intensity of the moderated positron flux is expected to be $10^9/s$, which will make the positron beam one of the most intense ones in the world. A general review of intense beams, including the linac-based positron beams and reactor-based positron beams, applied around the world will be given. The details of the MIPBF project, especially the defect characterization system will be discussed in the thesis. A beam system for out of core test of the defect characterization system has been constructed. Components in spectrum acquisition and analysis system have been calibrated and tested. A simple coincidence Doppler broadening spectroscopy system has been set up. An electron beam for simulating the positron beam has been tested successfully. The experiments on beam transportation will be discussed. A new positron source and a moderator have been installed in the beam system. The operational procedures and instructions of the beam system will be provided.

Acknowledgements

I would like to express my sincere gratitude to my supervisor, Dr. Peter Mascher, for his expertise, understanding, and patience. Without his support, I would never be able to accomplish this work. I would like to thank Dr. Peter Simpson who always encourages me to explore more on the path of research. Dr. Simpson not only generously shared his experiences and resources with me, but also was always ready to answer my questions. I also would like to thank Dr. Andy Knights, for his efforts in coordinating the MIPBF project.

I would like to thank Jacek Wojcik, who offered me great help in the work both in McMaster and Western. Thanks to Zhilin Peng for helping me get used to the life in Canada. I would like to thank Doris Stevanovic for her solicitude in my daily time. I would also like to thank our group members, Zahra Khatami and Bomi Lee, for sharing their experiences with me.

Finally, I would like to thank my parents for their unconditioned love and encouragement. I would also like to thank my girlfriend, Ai Ye, who provided me support and inspiration during my hard times.

Contents

Chapter 1 - Introduction	1
Chapter 2 – Positron Theory	3
2.1 Conventional positron sources	11
2.2 Positron annihilation lifetime spectroscopy (PALS)	15
2.3 Doppler broadening spectroscopy (DBS)	19
2.3.1 Conventional Doppler broadening spectroscopy	19
2.3.2 Coincidence Doppler Broadening Spectroscopy (CDBS)	23
2.4 Positron Beams	27
2.4.1 Moderators	28
2.4.2 Positron Traps	33
Chapter 3 – Intense Positron Beams.....	37
3.1 Linac based positron beams.....	37
3.1.1 Linac-based positron beam at AIST (Japan)	38
3.1.2 Linac-based positron beams in other countries	41
3.2 Reactor based positron beams	43
3.2.1 POSH.....	44
3.2.2 NEPOMUC	47
3.2.3 PULSTAR	49
3.2.4 KUR and HIPOS.....	51
Chapter 4 – The McMaster Intense Positron Beam Facility (MIPBF) Project	54
4.1 MIPBF Overview	54
4.2 Spectrum acquisition and analysis system	58
4.2.1 Detector performance test	60
4.2.2 Coincidence setting.....	67
4.3 Positron beam system.....	74
4.3.1 Overview	74
4.3.2 Software description.....	79
4.4 Operation of the system	83

4.4.1 Vacuum procedure.....	83
4.4.2 Shielding for radiation and high voltage.....	85
4.4.3 Beam transportation.....	87
4.4.4 Moderator preparation and installation.....	93
4.4.5 Source installation.....	94
4.4.6 Search for the positron beam	97
4.4.7 Ion beam and temperature control	101
Chapter 5 - Summary and Prospects	105
5.1 Summary	105
5.2 Future work.....	105
Bibliography	107
Appendix A	111

List of Figures

Figure 2. 1 e ⁺ -e ⁻ pair production from high energy electrons.....	5
Figure 2. 2 Positron diffusion process in a solid ^[4]	7
Figure 2. 3 The methods of positron annihilation technique.....	9
Figure 2. 4 Decay of ²² Na.....	13
Figure 2. 5 Schematic of a typical fast-fast coincidence PAL Spectroscopy system.....	16
Figure 2. 6 Electronics for a positron lifetime system (From left to right: CFDD, Fast Coincidence, CFDD, TAC, MCA, Amplifier and two High voltage power supplies, respectively)	18
Figure 2. 7 Schematic of a recently acquired positron lifetime system ^[5]	18
Figure 2. 8 Doppler Broadening spectroscopy system.....	20
Figure 2. 9 S and W parameter in a Doppler broadening spectrum ^[9]	21
Figure 2. 10 2D Doppler broadening spectrum ^[9]	26
Figure 2. 11 CDB Spectrum after diagonalization compared with single detector spectrum ^[9]	27
Figure 2. 12 The comparison of energy spectrum of positrons from a ⁵⁸ Co source before and after moderation ^[11]	29
Figure 2. 13 The structure of an N ₂ moderated source ^[13]	31
Figure 2. 14 The first three stage positron trap ^[14]	34
Figure 2. 15 Four stage positron trap ^[15]	35
Figure 2. 16 Energy spread of a positron pulse from the trap developed by Gilbert et al. ^[16]	36
Figure 3. 1 Positron production and moderation in the positron beam at AIST.....	39
Figure 3. 2 Layout of the positron beam system at AIST ^[18]	40
Figure 3. 3 PALS result using a Positron Probe Microanalyzer	41
Figure 3. 4 The 1997 configuration of the positron source of POSH. ^[32]	45
Figure 3. 5 Decrease of beam intensity with time	46
Figure 3. 6 S parameter of tungsten foils. The data are shown for tungsten foils: used in the POSH source for 3 years (R1-R5); as rolled; annealed for 7 hours at 1700K in vacuum. ^[34]	47
Figure 3. 7 Structure of the positron source tube in NEPOMUC ^[37]	49
Figure 3. 8 The layout of the slow positron beam in PALSTAR reactor ^[39]	50
Figure 3. 9 Schematic drawing of HIPOS positron generator ^[41]	52
Figure 3. 10 Top view of the positron beam line and the material irradiation chamber at KUR ^[42]	53
Figure 4. 1 Layout of the MNR.....	55

Figure 4. 2 Model of the positron source tube at MNR ^[43]	57
Figure 4. 3 Schematic of the CDBS set-up	60
Figure 4. 4 User interface of MAESTRO.....	61
Figure 4. 5 ²² Na energy spectrum from Detector 1	62
Figure 4. 6 ²² Na energy spectrum from Detector 2	63
Figure 4. 7 ¹³⁷ Cs energy spectrum from Detector 1	64
Figure 4. 8 ¹³⁷ Cs energy spectrum from Detector 2	65
Figure 4. 9 ¹³⁷ Cs energy spectrum from detector 1 with more counts.....	66
Figure 4. 10 ¹³⁷ Cs energy spectrum from Detector 2 with more counts.....	66
Figure 4. 11 Operational principle of a CFDD.....	68
Figure 4. 12 Energy spectrum based on the voltage range on discriminator.....	70
Figure 4. 13 Single detector coincidence	71
Figure 4. 14 Randomly collected spectrum.....	72
Figure 4. 15 (1)(2)(3)(4) are coincidence spectra with delays from 1 to 4 μs.....	73
Figure 4. 16 The current positron beam facility at Western University.....	75
Figure 4. 17 Original source chamber.....	76
Figure 4. 18 New defect characterization system.....	76
Figure 4. 19 The structures inside the sample chamber ^[44]	78
Figure 4. 20 Beam imaging system.....	79
Figure 4. 21 Vacuum control page.....	80
Figure 4. 22 Magnets page	81
Figure 4. 23 Plot page	82
Figure 4. 24 Top view of the defect characterization system in the cage ^[44]	86
Figure 4. 25 Electron gun.....	88
Figure 4. 26 Energy analyzers.....	89
Figure 4. 27 Beam transportation.....	90
Figure 4. 28 Shape on the screen (1) “milky way” (2) real beam spot.....	92
Figure 4. 29 Aluminum film on the sample holder to collect the beam current.....	92
Figure 4. 30 Moderator assembly (the moderator foil in the picture is broken).....	94
Figure 4. 31 Schematic of the source container	95
Figure 4. 32 Schematic of scintillator detector electronics	100
Figure 4. 33 Modified schematic for scintillator detector electronics.....	101
Figure 4. 34 Top view of the ion beam connected to the sample chamber ^[44]	103

List of Tables

Table 2. 1 Basic physical properties of positrons and electrons	4
Table 2. 2 Positron distribution in depth	8
Table 2. 3 Properties of positron emitting nuclei	12
Table 2. 4 Properties of some metals that can be used as moderators	30
Table 2. 5 Comparison of solid neon moderator and tungsten moderator ^[13]	32
Table 4. 1 Comparison of the parameters of four reactor based positron beams.....	56
Table 4. 2 Energy resolution of HPGe detectors measured with a Co-60 source at the 1.33MeV peak	62
Table A. 1 Count rate with the change of the scale on discriminator	111

Chapter 1 - Introduction

Positron techniques have been developed and applied in many different fields including but not limited to medicine, biology, physics and energy. The research in the laboratories with positron beams is involved in studies that range from fundamentals to applications such as electron–positron interactions, anti-hydrogen formation, modelling of astrophysical processes, and solid state material surface analysis. The intensity of the beam has become a bottleneck for the further development. In recent years, the development of nuclear reactor based positron beams succeeded to increase the intensity of positron beams from the $10^6/s$ level for conventional positron sources to the $10^9/s$ level, which made new research and applications possible. The McMaster Intense Positron Beam Facility (MIPBF) is a recently launched project based on the McMaster Nuclear Reactor (MNR) and aims to set up the first intense positron beam facility in Canada. The final intensity of the moderated positron beam is expected to be $10^9/s$, which will make the beam one of the most intense in the world. The MNR is a light-water swimming-pool-type research reactor located on the campus of McMaster University, and is one of the few research reactors still in operation in North America.

This work aims to provide a summary of the MIPBF project. In Chapter 2, a review of the fundamental theory of positron annihilation techniques is provided, as well as the composition of positron annihilation lifetime spectroscopy (PALS) systems, Doppler broadening spectroscopy (DBS) systems and positron beams. The current status of the intense positron beams, especially the reactor based intense positron beams around the world is reviewed in Chapter 3. The differences and similarities of the beams currently running or under construction are presented. Chapter 4 provides the detailed information of the McMaster Intense Positron Beam Facility (MIPBF) project, including the layout of the facility, and descriptions of system testing and operation procedures. In Chapter 5, a plan of future work to prepare for the experiments and improve the performance of the system will be provided.

Chapter 2 – Positron Theory

The existence of the positron was theoretically predicted by P. Dirac in 1930^[1] and experimentally confirmed by C.D. Anderson in cosmic radiation in 1932^[2].

The positron is the anti-particle of the electron, with the same overall properties except for the positive charge. When a positron encounters an electron, the pair will annihilate and emit 2 or 3 gamma rays. By detecting and analyzing the properties of these emission photons, information about the annihilation process can be obtained. The positron annihilation technique has been applied in solid state physics and has been developed rapidly since the 1960s. It has been playing an important role in material science, especially in the study of defects and phase changes as the micro-structure of a material can be probed. As a non-destructive detection technique, positron annihilation is a sensitive tool to study the micro-structure and the charge and electron momentum distribution in metals, semiconductors and polymers.

In addition to directly annihilating with electrons, positrons can form a bound state with electrons similar to a Hydrogen atom, which is called positronium (Ps). The energy at each energy level of Ps, which has a binding energy of -6.8eV and radius of $2a_0$, is half that of Hydrogen atom.

The positron is a lepton, with a spin of $\frac{1}{2}$. It obeys Fermi-Dirac statistics and can participate in the electromagnetic interaction, gravity and weak interactions, but does not participate in the strong interaction. Basic properties of positrons and electrons are shown in Table 2.1.

Table 2. 1 Basic physical properties of positrons and electrons

	Positron	Electron
Mass	9.1×10^{-31} kg	9.1×10^{-31} kg
Charge	$+e$	$-e$
Spin	$1/2$	$1/2$
Magnetic moment	$+1$	-1

The positron is an antiparticle and it will annihilate with an electron. Therefore it does not exist in nature. We produce it mainly in two ways. The first one is from the decay of radioactive isotopes. In the decay process of the radioactive isotopes, such as ^{22}Na , ^{64}Cu and ^{58}Co , a proton decays into a neutron and a positron. Those nuclides can be produced from nuclear reaction. Another way is to produce positrons by high energy (MeV) photons through the positron-electron pair effect as shown in Fig 2.1. For example, when high energy electrons from a linear accelerator hit a tungsten target, gamma rays will be produced by bremsstrahlung. Some gamma

rays with energy larger than 1.022MeV can turn into a positron and an electron. This reaction normally happens near a nucleus with high atomic number.

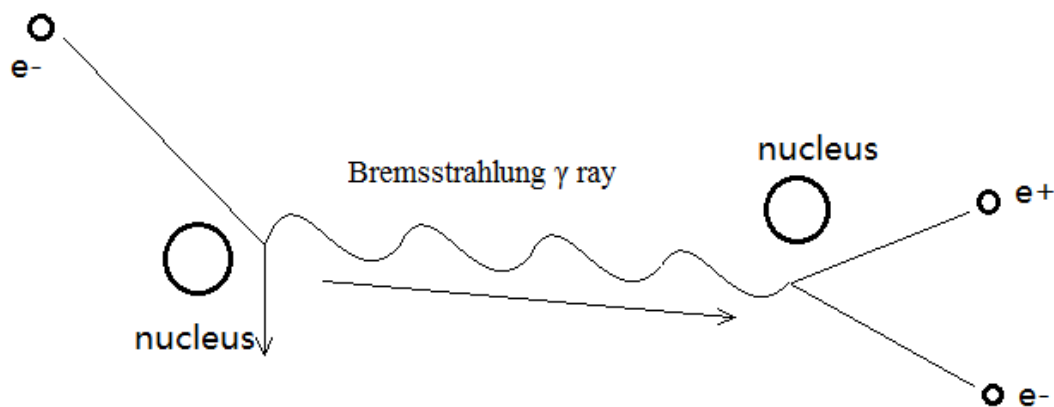


Figure 2. 1 e^+e^- pair production from high energy electrons

When the speed of a positron, v is much lower than the speed of light c ($v \ll c$), the energy equivalent of the mass of the positron and electron together is 1.022MeV , and the momentum of the gamma rays in sum will be almost zero. In the annihilation process, the number of photons produced is not fixed. However, based on energy and momentum conservation, the result of two gamma rays going in opposite directions with energy of 0.511MeV each has the highest possibility (378 times that of 3 gamma annihilation). In this way, the parameters related to 2-gamma-annihilation are the most important information in positron spectrum analysis. Based on the Dirac's work ^[3], when the relative speed v between the

positron and electron is far less than the speed of light c ($v \ll c$), the rate λ of 2-gamma-annihilation can be calculated by the following:

$$\lambda = \pi r_0^2 c n_e \quad (2.1)$$

In equation (2.1), n_e is the electron density at the location where the positrons annihilate, r_0 is the classical radius of the electron and c is the speed of light. This means that the annihilation rate is proportional to the electron density. Therefore, the positron can be used as a probe to detect the electron distribution in a material.

When the positron enters a material, the process is shown in Figure 2.2. Because of its positive charge, it will be repulsed by the nuclei. The positrons will lose energy in several inelastic scattering processes (electron ionization, electron-hole pair excitation, electron-phonon scattering) and slow down until reaching thermal energy. This process is called thermalization and it will take about several ps, which is much shorter than the lifetime of thermalized positrons in a solid (several hundred ps). Thermalized positrons will be in thermal equilibrium with the surrounding lattice and diffuse in a way that can be described by the Boltzmann equation. In this process, some positrons will interact with the defects in the solid and be trapped in a localized state. At last, positrons will annihilate with electrons and radiate γ -rays.

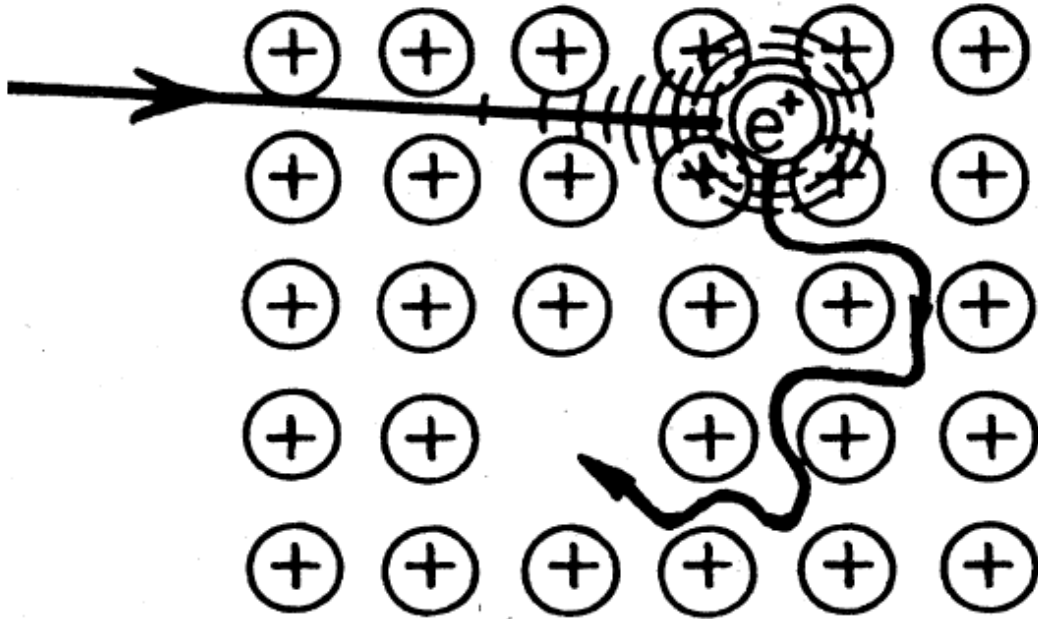


Figure 2. 2 Positron diffusion process in a solid ^[4]

Normally, the source used in a conventional laboratory to obtain positrons is from radioactive isotopes. The energy of positrons ranges from several hundred keV to several MeV. For example, the energy of positrons from ^{22}Na ranges from 0 to 545keV. The depth distribution where the positrons stop in materials is related to the energy of the positrons. If the positron travel length is R_+ and the absorption coefficient of the material to positron is α_+ , then $R_+=1/\alpha_+$ (cm^{-1}). For most materials, the experimental results of the absorption coefficient could be obtained by the following formula:

$$\alpha_+ \approx 17 \frac{\rho}{E_{\max}^{1.43}} \quad (2.2)$$

In equation (2.2), ρ is the density of the material (g cm^{-3}), and E_{\max} is the maximum energy of positron from the source (MeV). The depth in most materials

ranges from $10\mu\text{m}$ to 1mm . For a ^{22}Na source, when the density of material is $1\text{g}/\text{cm}^3$, the depth distribution is shown in Table 2.2,

Table 2. 2 Positron distribution in depth

Stopped e^+ (%)	Depth
0	$25\mu\text{m}$
90	0.6mm
99	1.1mm
99.9	1.7mm

It can be seen from the Table that, with normal sources, the positron can only work as a bulk probe. Only with lower energies variable between $0\sim 30\text{keV}$, the positron can be used in surface or thin film research.

The process from the creation of a positron in the ^{22}Na source to the thermalization and annihilation into 2 gamma rays is shown in Figure 2.3.

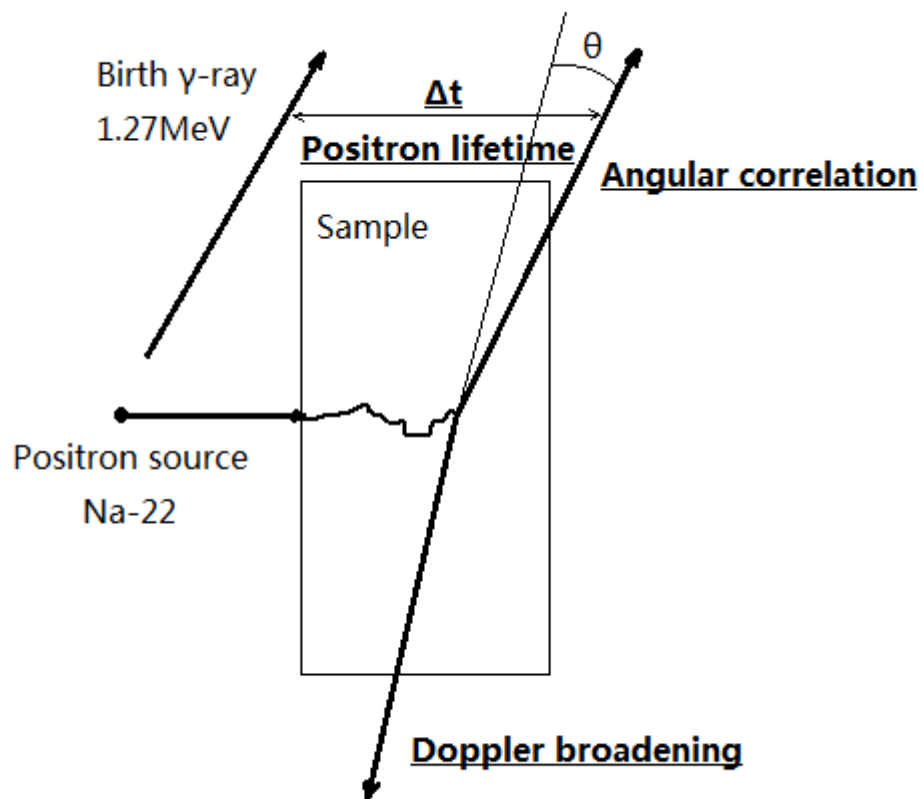


Figure 2. 3 The methods of positron annihilation technique

When the annihilation takes place, the energy of the positron is only 0.025eV at room temperature. In the material, the energy of the electron annihilating with a positron is several eV. Compared with 511keV, this is negligible. In the positron lifetime spectrum technique, ^{22}Na is the most widely used source in laboratories. The 1.28MeV gamma rays that set off with positrons are collected as the start signal, and the 511keV annihilation gamma ray is collected as the stop signal. The time period between the two signals is the lifetime of a positron. Positron lifetime τ is

inversely proportional to annihilation rate λ , and is inversely proportional to the electron distribution density. Therefore, the positron lifetime directly reflects the electron density at the location where positrons annihilate. This provides very useful information in defect studies of solids. In metals, for example, vacancy-type defects usually come with negative charges and can easily trap positrons. The density of electrons in defects is lower than that in the bulk. As a result, the positron lifetime is longer in the defects than in the bulk. Additionally, the bigger the defect is, the longer the positrons live.

The angular correlation of annihilation radiation (ACAR) is one of the commonly used techniques. Based on the conservation of energy and momentum, the direction of two annihilation gamma rays will not be exactly collinear, because of the electron momentum. The slight angle $\theta_{x,y}$ between the two gammas can be described by the following formula:

$$\theta_{x,y} = \frac{p_{x,y}}{m_0 c^2} \quad (2.3)$$

$p_{x,y}$ is the momentum component of one gamma photon perpendicular to the direction of another gamma photon; m_0 is the mass of an electron and c is the speed of light. By detecting and analyzing the small angle, the distribution of electrons in the solid can be obtained.

Another important application of positron annihilation is Doppler broadening spectroscopy. The momentum of positrons and electrons before annihilation can

lead to Doppler energy shifts of the annihilation γ rays. The total momentum of the positron-electron pair along the x-axis is denoted by P_x , which can be calculated by $P_x = Mv_x$ ($M=2m$, is the total mass of the particles, and v_x is the speed along the x-axis). For a moving light source, if the frequency along the x-axis is denoted by ν , the observed frequency shift will be obtained by the following equation:

$$\frac{\Delta\nu}{\nu} = \frac{v_x}{c} \quad (2.4)$$

The energy of the annihilation γ ray is E_γ , which is equal to $h\nu$ (h is Planck's constant). The Doppler broadening ΔE is obtained by equation (2.5) in the following:

$$\Delta E = h\Delta\nu = \frac{E_\gamma v_x}{c} = E_\gamma \frac{P_x}{2mc} = \frac{cP_x}{2} \quad (2.5)$$

The energy of thermalized positrons is about 0.025eV, and the energy of electron is about several eV. The energy and momentum of positrons is thus relatively negligible. The total energy and momentum depend on the electron. With high purity Ge detectors of resolution better than 2keV, the electron momentum information can be analyzed from the Doppler broadening.

2.1 Conventional positron sources

There are many kinds of radioactive nuclei that can produce positrons. The selection of the source needs to be based on both the requirement of experiment and

the property of the source. Some information on the nuclei is listed in the following

Table 2.3:

Nucleus	Half-lifetime $T_{1/2}$	β^+ maximum energy $E_{max}(\text{MeV})$	Reaction to produce nucleus
^{22}Na	2.6a	0.545	$^{24}\text{Mg}(d,\alpha)^{22}\text{Na}$
^{64}Cu	12.8h	0.653	$^{63}\text{Cu}(n,\gamma)^{64}\text{Cu}$
^{68}Ge	288d	1.89	$^{66}\text{Zn}(\alpha,2n)^{68}\text{Ge}$
^{58}Co	71d	0.474	$^{58}\text{Ni}(n,p)^{58}\text{Co}$
^{44}Ti	47.3a	1.47	$^{45}\text{Sc}(p,2n)^{44}\text{Ti}$
^{11}C	20.4min	0.96	$^{14}\text{N}(p,\alpha)^{11}\text{C}$

Table 2. 3 Properties of positron emitting nuclei

Among those nuclei, ^{22}Na is most widely used in materials research. It has some advantages over other sources: a relatively long half-lifetime that ensures the stability of positron flux during the experiment; a 1.28MeV γ ray emitted virtually

simultaneously with the positron that can act as the start signal for lifetime measurement. For medical uses such as Positron Emission Tomography (PET), however, some light elements are commonly used such as ^{11}C . For one thing, their short lifetime will not cause too much damage on the human body; for another, the elements will be absorbed and utilized by body.

The decay of ^{22}Na is shown in Figure 2.4, in which ^{22}Na decays into $^{22}\text{Ne}^*$ and emits a positron. The lifetime of the excited state $^{22}\text{Ne}^*$ is about 3ps. After that, it will decay to the steady state and emit a 1.28MeV γ ray. Compared with the lifetime of a positron, the lifetime of the excited state $^{22}\text{Ne}^*$ is negligible. As a result, it is normally concluded that the 1.28MeV γ ray is created at the same time as the positron.

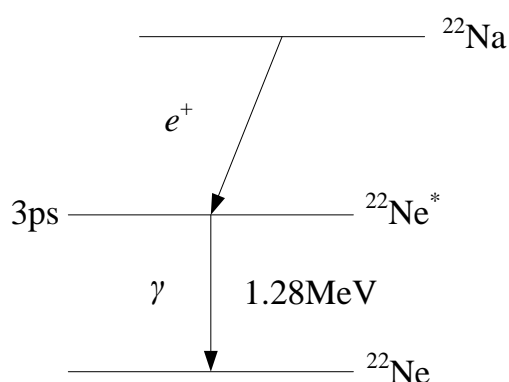


Figure 2. 4 Decay of ^{22}Na

For a conventional experiment, ^{22}Na exists in the form of $^{22}\text{NaCl}$. One puts one or more drops of the $^{22}\text{NaCl}$ solution on a metal or polymer film with a dropper, then dries the solution with an infrared lamp and puts another piece of film on it. The source needs to be sealed before use. Sometimes, a metal frame can be fixed around the source to strengthen it, as well as enable the source to be used in extreme conditions such as high temperature and high vacuum. The intensity of the source normally ranges between 10 and 50 μCi .

In the experiment, samples and sources are placed in a sandwich structure, that is, two “identical” samples sandwich the source to ensure that most positrons annihilate in the samples. Also, the thickness of the samples should be larger than the maximum positron penetration depth.

The maximum positron penetration depth can be calculated with the following equation:

$$\frac{1}{R_+} = \frac{2.8 \times \rho \times Z^{0.15}}{E^{1.19}} \quad (2.6)$$

In equation (2.6), E is the theoretical average positron kinetic energy from ^{22}Na , about 0.15 MeV; R_+ is the positron penetration depth; Z is the atomic number of the material and ρ is the density of the material. For metals and other “hard” materials,

the penetration depth is about 0.3~1mm. For polymers with lower density, this depth is about 1~2mm.

2.2 Positron annihilation lifetime spectroscopy (PALS)

A conventional positron annihilation lifetime spectroscopy system can be configured in two different ways: fast-fast coincidence and fast-slow coincidence PALS. The structure of a fast-slow coincidence PALS system is relatively complex and the count rate is relatively low. Therefore, it was mainly used in the early stages of development and has been gradually eliminated with the advancement of experimental techniques and theory. The most widely used configuration nowadays is the fast-fast coincidence system. A Schematic of the spectroscopy system is shown in Fig. 2.5. Two sets of fast-fast coincidence spectroscopy systems have been in operation since the 1990s in the conventional positron lab at McMaster University.

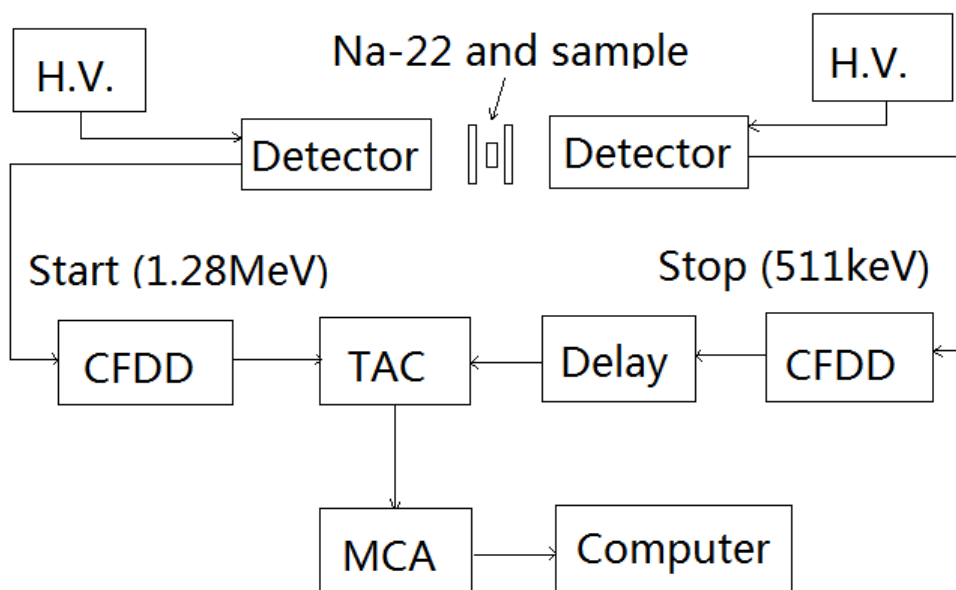


Figure 2. 5 Schematic of a typical fast-fast coincidence PAL Spectroscopy system

The positron lifetime system shown in Fig. 2.5 includes two high voltage power supplies, two scintillator detectors, and two constant fraction discriminators (CFDD), a Time-to-Amplitude Converter (TAC), a Delay Box and a Multi-Channel Analyzer (MCA). The constant fraction discriminators are used to select the energy and time of pulses. By adjusting the upper and lower level thresholds, the energy window can be determined. The start channel only allows the pass of the pulses with 1.28MeV energy and the stop channel only allows the pass of the pulses with 0.511MeV energy. The Time-to-Amplitude Converter can select start and stop

signal from an annihilation event and convert the time duration between two signals to a voltage. Then the voltage signal is imported into the Multi-Channel Analyzer to generate the positron lifetime spectrum. Normally, ^{22}Na used as the positron source and in a conventional lab it is relatively weak (below $10^6/\text{s}$), which means the average interval between two positron emitting events is longer than $1\ \mu\text{s}$. This interval is much larger than the collection time of the Time-to-Amplitude Converter (TAC). Thus in this setting, the Time-to-Amplitude Converter can also have the function of timing coincidence.

The conventional positron lab at McMaster purchased a new PAL spectroscopy system in 2014, as is shown in Fig. 2.6. Compared with the original systems, this new PALS system includes a Fast Coincidence unit. The layout of the new PALS system is shown in Fig. 2.7. The signal from the 414 Fast Coincidence unit is input into the TAC as a gate signal. This setting is helpful to both improve time resolution and reduce noise. The time resolution is an important parameter to reflect the quality of a scintillator detector. The time resolution of this system is guaranteed to be no worse than 200 ps, which is a desirable value for PAL experiments.

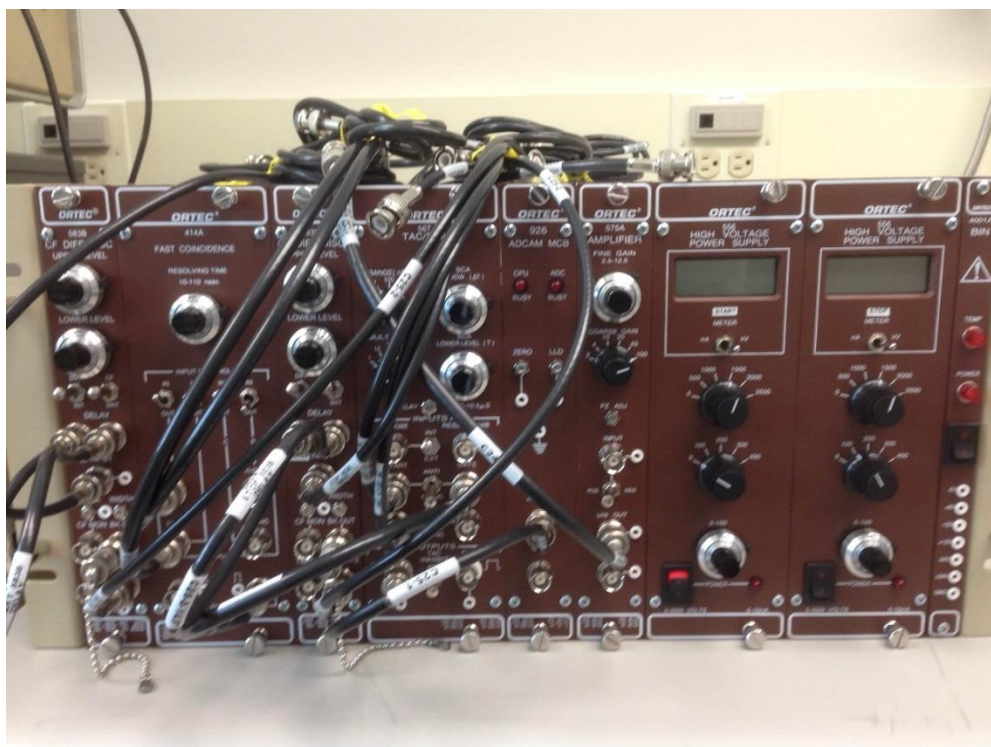


Figure 2. 6 Electronics for a positron lifetime system (From left to right: CFDD, Fast Coincidence, CFDD, TAC, MCA, Amplifier and two High voltage power supplies, respectively)

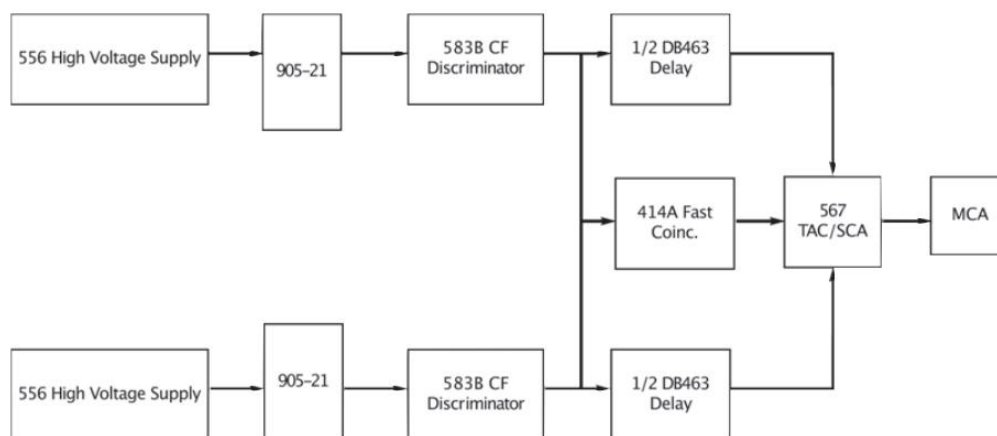


Figure 2. 7 Schematic of a recently acquired positron lifetime system [5]

2.3 Doppler broadening spectroscopy (DBS)

2.3.1 Conventional Doppler broadening spectroscopy

The detector used in the measurement of a Doppler broadening spectrum is a high purity Ge (HPGe) semiconductor detector with high energy resolution, as is shown in Fig. 2.8. This type of detector should be kept at a low temperature during operation by using liquid nitrogen cooling. The sample-source sandwich structure for this measurement is the same as in a positron lifetime measurement, i.e., sample-source-sample. The signal from the detector is amplified by the amplifier and then input into a multichannel analyzer. The γ energy spectrum can then be collected. The count rate of Doppler broadening measurements is about two orders of magnitude higher than angular correlation measurement of positron annihilation radiation. Despite the benefit of high count rate, the system has its shortages, for example, low energy resolution. Nowadays, a HPGe detector in a good condition can achieve an energy resolution of 1keV at 511keV. It is one magnitude less than angular correlation measurement.

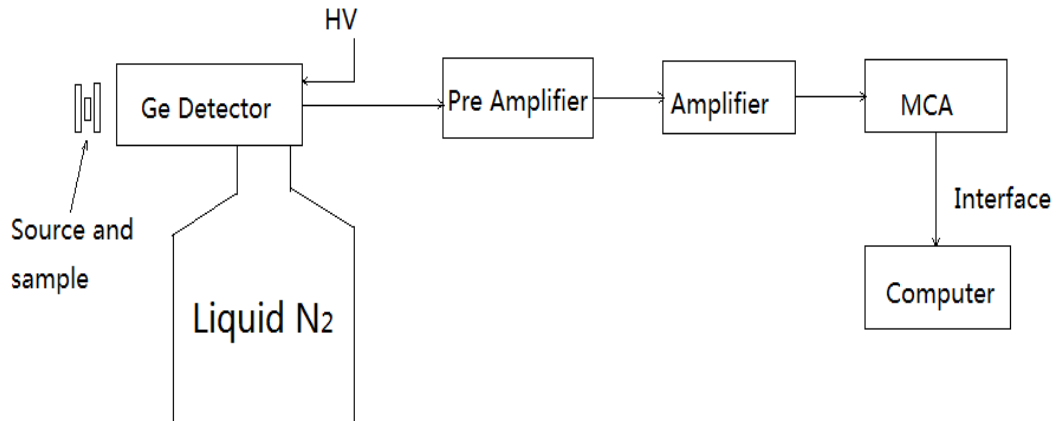


Figure 2. 8 Doppler Broadening spectroscopy system

To reduce the effect of low resolution, two parameters are normally defined for the Doppler broadening spectrum to be analyzed, the S parameter and the W parameter. As is shown in Fig. 2.9, the S parameter is defined as the ratio of the area A in the center of the peak and the total area under the spectrum, while the W parameter is defined as the ratio of the total area B on two wing regions of the peak and the total area of the spectrum. The two parameters can be described by the following equation:

$$S = \frac{A}{SUM}, \quad W = \frac{B}{SUM} \quad (2.7)$$

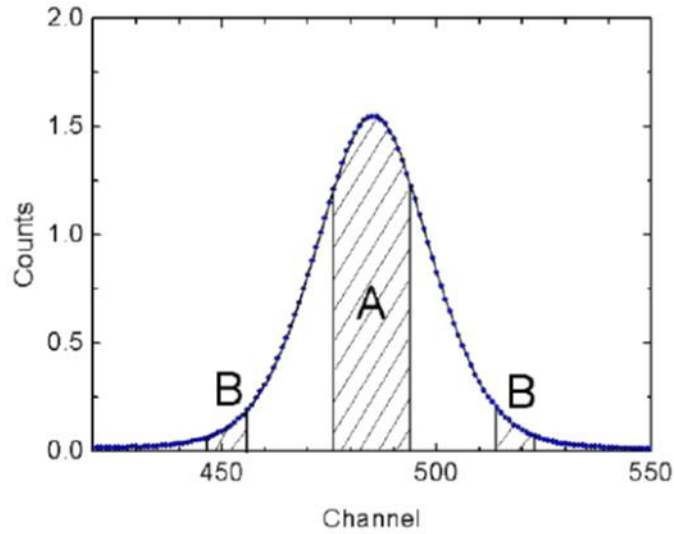


Figure 2.9 S and W parameter in a Doppler broadening spectrum^[9]

Fig 2.9 describes the regions of the S and W parameters. From the Doppler energy shift ΔE , which can be calculated by $\Delta E = cP_1/2$, the S parameter refers to the momentum information of outer shell electrons and the W parameter refers to the momentum information of inner shell electrons. When positrons are captured by defects in a material, the probability of the positrons to annihilate with high energy inner shell electrons is decreased and the probability to annihilate with outer shell electrons is increased. Thus, the S parameter will increase and the W parameter will decrease. Based on the change of these two parameters, information about defects can be obtained.

Before analyzing the spectrum, the background counts need to be subtracted. Because of effects such as the Compton Effect of the 1,275keV and 511keV γ rays,

the background counts in the low energy region are higher than in the high energy region. As a result, the background cannot be subtracted linearly. Mogensen etc.^[6] described a way to subtract the background of a Doppler broadening spectrum:

$$B_i = B_h + (B_l - B_h)A_i / A_t \quad (2.8)$$

In equation (2.8), B_i is the total background, and B_l , B_h are average backgrounds levels in the low energy and high energy regions, respectively. A_i is the total number of counts before the i 'th channel in the spectrum and A_t is the total number of counts in the spectrum. With this method to subtract the background counts, the background on the two sides of the peak becomes almost symmetrical. Normally, either the S parameter or the W parameter needs to be analyzed to get the information of defects in material. In some cases, however, the species of defects as well as the chemical environments around the defects are important to study. For such studies, the S and the W parameters need to be analyzed in combination. Based on the positron capture model in defects, the S and the W parameters can be calculated by the following expression:

$$S = (1 - f)S_b + fS_d, \quad W = (1 - f)W_b + fW_d \quad (2.9)$$

Combing the two equations in (2.9) yields the following expression:

$$S = R \cdot (W - W_b) + S_b \quad (2.10)$$

In the above equations, S_b and S_d are the S parameter in the bulk and in defects, respectively, while W_b and W_d are the corresponding W parameters. It takes no effort to see that the parameter $R = (S_d - S_b)/(W_d - W_b)$ is only related to the species of defects, yet not related to the density of defects. We can thus use the S and the W parameters to create an S-W plot, that is, to plot a curve with S parameter vs. W parameter. If the data points locate on a straight line, it indicates that the specific nature of the defects remains the same. If the data points locate on several straight lines, it means that there are different species of defects present.

2.3 2 Coincidence Doppler Broadening Spectroscopy (CDBS)

Lynn *et al.*^[7] developed a coincidence Doppler broadening spectroscopy system with a Ge(Li) detector and a NaI detector placed face to face. After the coincidence of signals from two detectors, the peak-to-background ratio was improved to 4500:1, which is 30 times higher than that of a normal Doppler broadening spectrum. After that, they developed a coincidence Doppler broadening spectrometer

with two Ge(Li) detectors and obtained a two-dimensional spectrum^[8]. After a series of data processing procedures, the two-dimensional spectrum can be transferred to a one dimension spectrum. In this one dimensional spectrum, the peak-to-background ratio is increased by about 10^5 times and the energy resolution is increased by a factor of $\sqrt{2}$. Based on the excellent performance of coincidence Doppler broadening spectroscopy using two detectors, we can even identify the elements in the material using the spectrum.

The principle of Doppler broadening spectroscopy using two detectors can be described as follows. For two Ge detectors, the energy of the two gamma rays in the same event are E_1 and E_2 , then,

$$E_1 = m_0c^2 + cP_L/2 - E_b/2 \quad (2.11)$$

$$E_2 = m_0c^2 - cP_L/2 - E_b/2 \quad (2.12)$$

In the equations, m_0 is the mass of electron when it is in the stationary state, P_L is the total annihilation momentum of positrons and electrons along the axis of the detectors, E_b is the binding energy of electrons. The sum and difference can be defined as E_s and E_d , which can be calculated by the equations of $E_s = E_1 + E_2$ and $E_d = E_1 - E_2$, respectively.

Since the binding energy E_b is relatively very small, it is negligible compared to the energy of gamma rays. Then the difference can be described as

$$E_d = E_1 - E_2 = cP_L \quad (2.13)$$

Based on equation (2.13), the energy difference of the gamma rays detected by two detectors is two times that of the Doppler broadening. The signals of gamma rays from two detectors are amplified by the amplifiers and then are sent to an Analog-to-Digital Converter (ADC). The output signals from ADCs are separately sent to the X and Y inputs of a dual-input multichannel analyzer (MCA). At the same time, the output signals of the amplifiers are sent to two single-channel analyzers (SCA) and then input into a Fast Coincidence unit. After the discrimination by the single-channel analyzers, only the signals of the gamma rays with an energy around 511keV are picked out. Only when two detectors get the signals from the same event, the signals can be recorded. The result from a dual-input MCA is a 2D Doppler broadening spectrum as shown in Fig. 2.10.

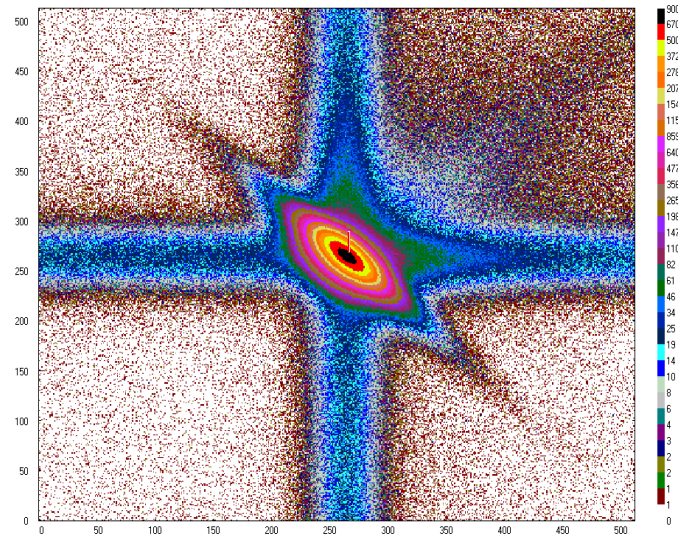


Figure 2. 10 2D Doppler broadening spectrum [9]

The projections of the 2D data along the X-axis and Y-axis are the Doppler broadening spectrum from each single detector. The sum of energy from two annihilation gamma rays is $E_1 + E_2 = 1.022\text{MeV}$. This fact can be used to additionally reduce the background. Every detector has its own energy resolution. Therefore, an energy range of $E_1 + E_2$ is selected. The energy range starts from 2 times the energy resolution before $1,022\text{keV}$ and stops at 2 times the energy resolution after $1,022\text{keV}$. By calculating the energy difference of each point on the 2D Doppler Broadening spectrum with formula (2.12), a new one-dimensional Doppler Broadening spectrum can be created. This spectrum is equivalent to the projection along the diagonal of $E_1 + E_2 = 1.022\text{MeV}$ in the 2D spectrum. This process is called diagonalization.

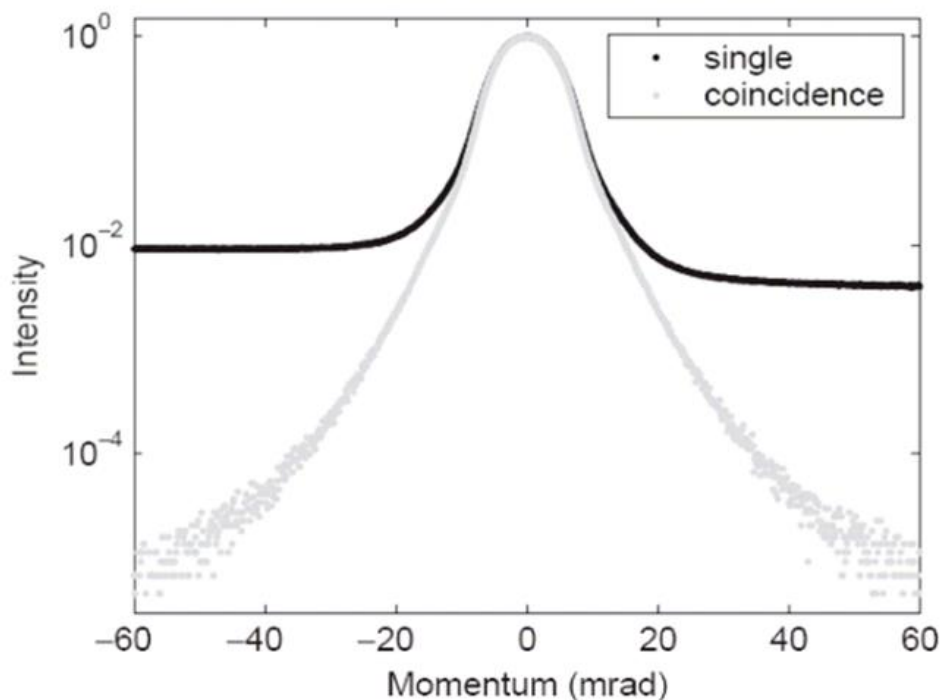


Figure 2. 11 CDB Spectrum after diagonalization compared with single detector spectrum^[9]

As is shown in Fig. 2.11, the 2D-CDB spectrum is substantially symmetrical and the peak-to-background ratio is greater than 10^5 , which is three orders better than in a conventional Doppler broadening spectrum. Additionally, the energy resolution is increased by $\sqrt{2}$ times.

2.4 Positron Beams

Positrons from the sources used in the conventional lab usually come with high energy and wide-spread energy range. They are only to be used to measure the

bulk defects in materials. Ever since the 1980s, new slow positron techniques have been developed. By controlling the energy of positrons, surface or near surface structures of materials can be examined. In addition, the positron source is far away from the samples. Therefore, the source will not pollute or affect the samples. Finally, since the energy of the positrons is low, the thickness of samples can be very thin.

2.4.1 Moderators

The idea to moderate positrons was first put forward by Madanskii in 1950^[10]. When positrons are injected into solids, which have negative work function, positrons will be thermalized in the solid. Then they will have a chance to diffuse out from the surface. Those positrons have very low energy (eV level), and the full width at half maximum (FWHM) of the energy spread can be as low as 50meV. The conversion efficiency can be 0.01. Compared with the positron flux in the same energy interval from the radioactive isotope, the positron flux after moderation can be six orders of magnitude higher. The difference of the positron energy spectrum before and after moderation can be demonstrated in the Fig. 2.12.

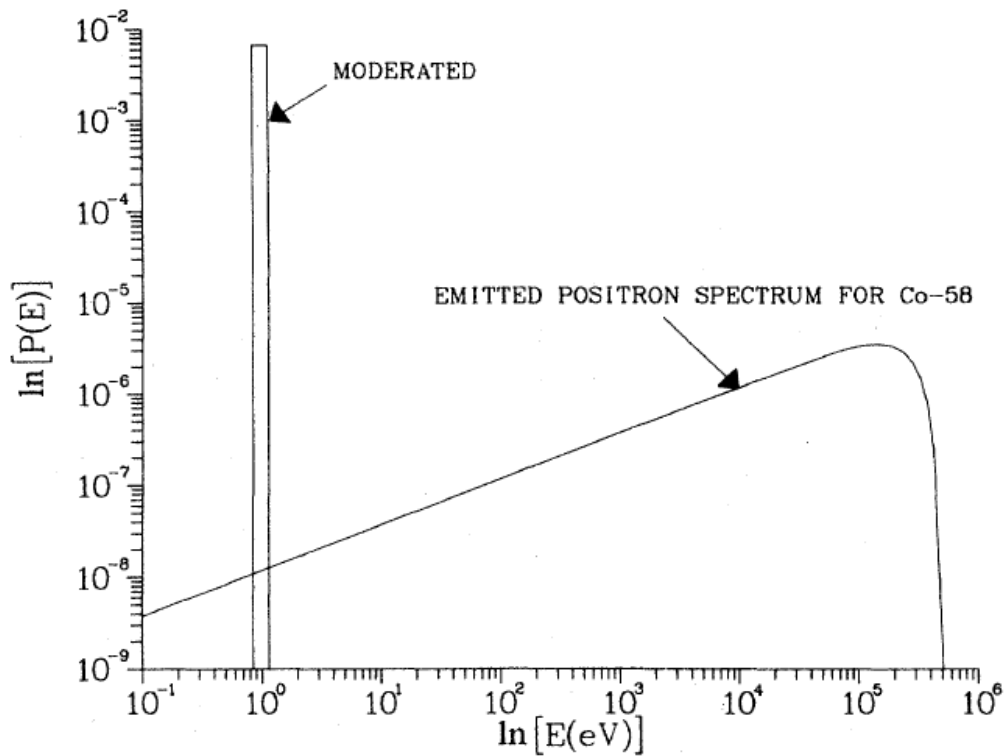


Figure 2.12 The comparison of energy spectrum of positrons from a ^{58}Co source before and after moderation ^[11]

The moderation efficiency is determined by three aspects: the depth distribution of the fast positrons; the percentage of the thermalized positrons that can diffuse to the surface; and the percentage of the positrons on the surface that can escape from the surface (P_{em}). The moderation efficiency can be calculated as follows:

$$\varepsilon = \frac{1.7P_{em}\rho(D_+\tau_{eff})^{1/2}}{(E_{max})^{1.14}} \quad (2.14)$$

In equation (2.14), ρ is the density of moderator (g cm^{-3}); D_+ is the positron diffusion coefficient ($\text{cm}^2 \text{s}^{-1}$); τ_{eff} is the lifetime of positrons in the moderator; and E_{max} is the maximum energy of the incident positrons.

A comparison of some metals available to work as a moderator is listed in Table 2.4. It shows that annealed crystal tungsten has the best moderation efficiency.

	Ni	Pt	Ta	W(100) as-received	W(100)in situ annealed
$\Phi^+(\text{eV})$	-1.5(2)	-2.2(2)	-1.6(6)	-2.5(2)	-3.00(5)
Relative e^+ yield	1.000(8)	0.665(7)	0.137(5)	1.180(9)	13.47(3)
Oxygen (at. %) ^a	7.9	9.2	7.0	38.5	-
Carbon (at. %) ^a	64.7	61.5	58.9	39.4	-

^a Rest to 100% is the metal substrate

Table 2. 4 Properties of some metals that can be used as moderators^[12]

After examining different kinds of materials, tungsten and noble gases are often selected as moderators. Tungsten is the most widely used moderator at present. It is easy to prepare and can reach a moderation efficiency of $10^{-4}\sim 10^{-3}$.

The process to prepare a noble gas moderator is different from that of metal moderators. Firstly, a small amount of noble gas is guided into the source chamber.

Then the temperature near the positron source is decreased to below the freezing point of the gas until the gas forms a thin layer of solid around the source. After that, the temperature is increased by several degrees to anneal the moderator. The structure used to grow a solid neon moderator is described in D. G. Greaves's work^[13], in which a ^{22}Na source was inserted into a parabolic copper cup mounted on an Elkonite rod attached to the second stage of a two-stage closed-cycle refrigerator. The temperature of the second-stage is typically 6-6.5K and the source temperature is about 1K higher.

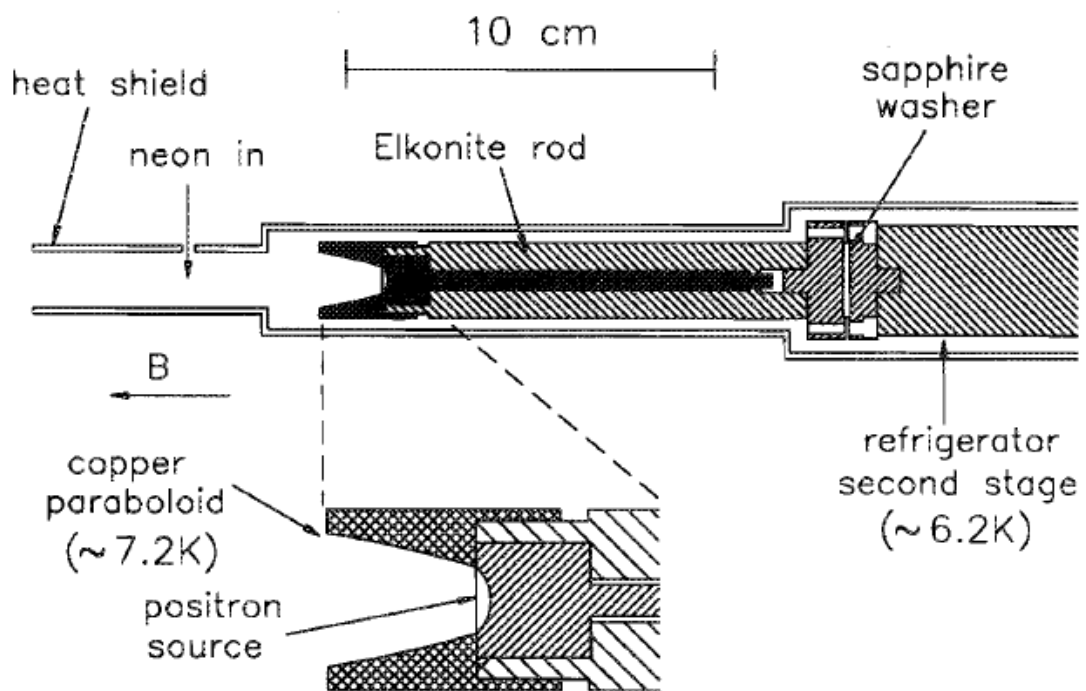


Figure 2. 13 The structure of an N₂ moderated source^[13]

The comparison of a rare gas moderator (Neon as an example) and tungsten is given in Table 2.5.

Table 2. 5 Comparison of solid neon moderator and tungsten moderator ^[13]

Parameter	Neon moderator	Tungsten Moderator
Source strength (mCi ²² Na)	65	150
Source efficiency (%)	19	19
Fast e ⁺ flux (s ⁻¹)	4.6×10 ⁸	1.0×10 ⁹
Moderated e ⁺ flux (s ⁻¹)	1.2×10 ⁷	1.0×10 ⁶
Efficiency ^a	0.005	2×10 ⁻⁴
Efficiency ^b	0.026	1×10 ⁻³
Energy spread (FWHM) (eV)	~1.8	~0.6
Trapping rate (s ⁻¹)	3.9×10 ⁶	4.0×10 ⁵
Trapping efficiency (%)	~30	~40
Positron lifetime (s) ^c	45	45
Positron lifetime (h) ^d	0.5	0.5
Total trapped positrons	1×10 ⁸	1.6×10 ⁷

a Relative to source strength

b Relative to emitted positrons

c With buffer gas, p~5×10⁻⁷ Torr

d At base pressure, p~5×10⁻¹⁰ Torr

Even though the moderation efficiency of a solid neon moderator is higher than that of tungsten, it bears some disadvantages. One of them is that the energy spread of the moderated positrons obtained from the rare gas moderators can be a

factor of two times larger than that obtained from tungsten moderators. Another disadvantage of solid gas moderators comes from their instability. The lifetime of the moderator depends largely on the temperature and vacuum under working conditions. Normally, the moderator needs to be regrown every seven days.

2.4.2 Positron Traps

Besides the moderation technique, another way of accumulating a large amount of positrons with variable energy was developed in 1988 by Surko et al.^[14]. The principle of this design is to have positrons interacting with N₂ gas and thereby slowing them down to room temperature. With differential pumping techniques and a specific electrode structure, a three stage trap is created as is shown in Fig.2.14.

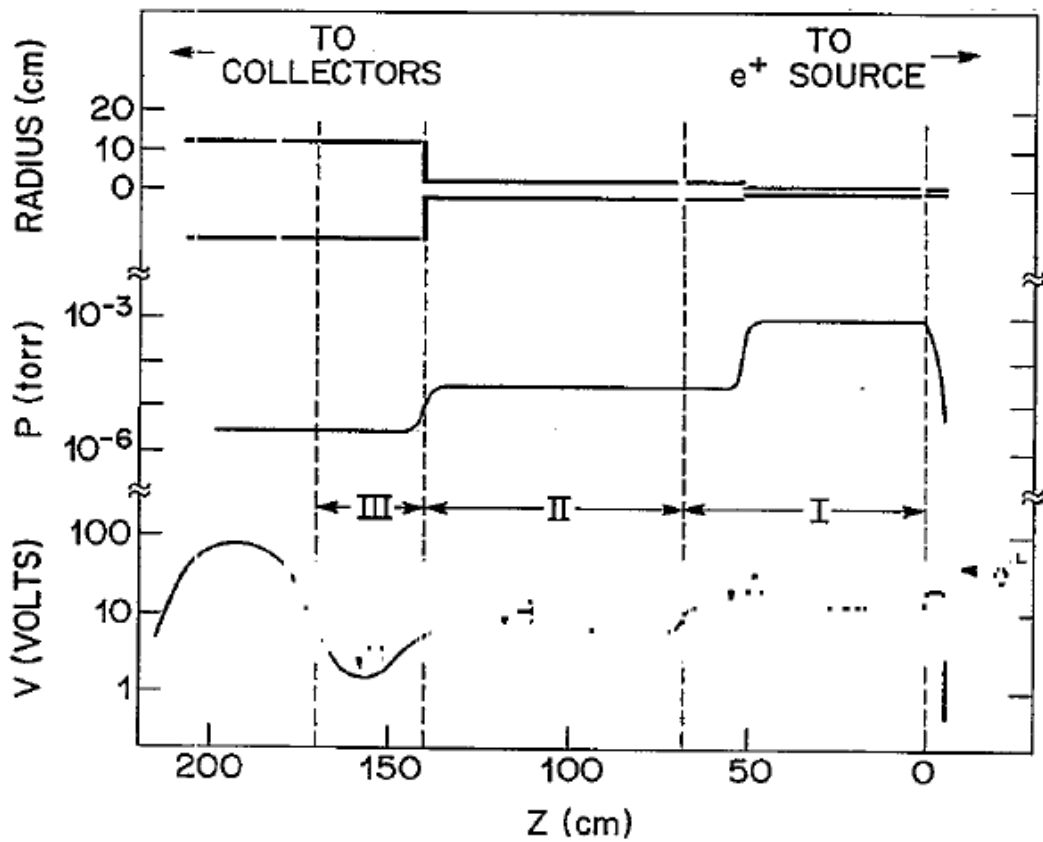


Figure 2.14 The first three stage positron trap^[14]

The pressure of N_2 gas in the three stages ranges from 10^{-6} to 10^{-3} Torr. Positrons lose energy by electronic excitation and ionization or by vibrational excitation of the N_2 . With an $86\text{mCi } ^{22}\text{Na}$ source and tungsten moderator, Surko *et al.*^[14] achieved to store a maximum of 3.3×10^5 positrons. Greaves *et al.*^[15] modified the design by adding a fourth stage as is shown in Fig. 2.15 in order to improve the measurement result.

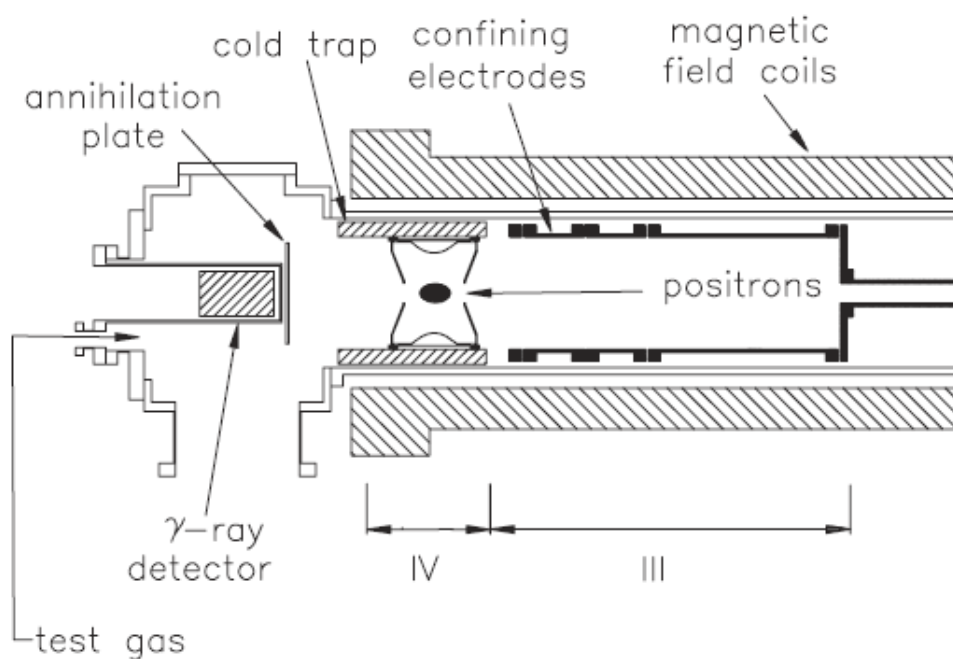


Figure 2. 15 Four stage positron trap^[15]

With the development of this technique, as many as 10^8 positrons can be stored. The accumulated positrons can be extracted by an electrode in a very short time to form a pulse containing a large amount of positrons. The energy spread of the pulsed positrons can reach 18meV (FWHM)^[16], as is shown in Fig 2.16, which is better than the energy spread of a positron beam from a moderator. This technique can be applied to the study of anti-hydrogen formation, positron inelastic scattering processes with molecules and atoms, and annihilation-rate measurements.

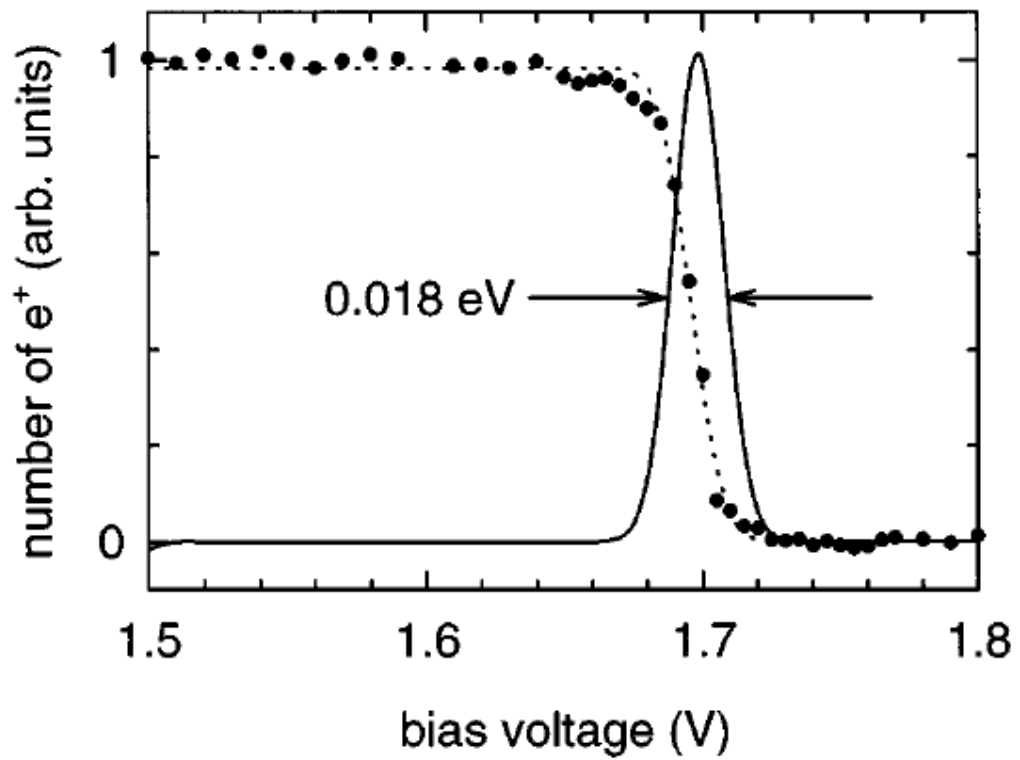


Figure 2. 16 Energy spread of a positron pulse from the trap developed by

Gilbert et al.^[16]

Chapter 3 – Intense Positron Beams

With the development of the positron beam technique, the intensity became the limitation to certain applications. With higher beam intensity, not only shorter measurement times can be achieved, but entirely new proposals can be envisaged, such as antimatter research. The intensity of the beam can be improved by increasing the activity of the source or by increasing the moderation efficiency. As discussed before, researchers have succeeded in getting the moderation efficiency up to 1%. To increase the source intensity, two different ways have been developed: pair production by nuclear reactor based sources and pair production by accelerator facilities, especially by linear electron accelerators (LINAC).

3.1 Linac based positron beams

Accelerator-based positron sources can produce much higher positron intensity compared to isotope-based sources. High energy electron beam from a linac is guided to a target to produce bremsstrahlung. Then positrons are created from positron-electron pair production in a converter. Several LINAC-based slow positron beams are in operation at linacs in Japan, China, USA, Germany and France.

3.1.1 Linac-based positron beam at AIST (Japan)

The positron beam at the Advanced Industrial Science and Technology (AIST) laboratory is a linear accelerator based slow positron facility, which is located in Tsukuba, Japan. The positron beam is mainly used to study materials using the positron micro-beam technique. As is shown in Fig. 3.1, the positrons are created by pair production by bremsstrahlung. An electron beam from a linac with an energy of 70 MeV hits a Ta converter target to produce gamma rays. Then the gamma rays produce fast positrons by positron-electron pair production. The positrons produced by pair production are normally in the energy range keV-MeV. The fast positrons are immediately moderated through a set of 25 μm thickness tungsten films and are emitted as slow positrons with eV level energy.

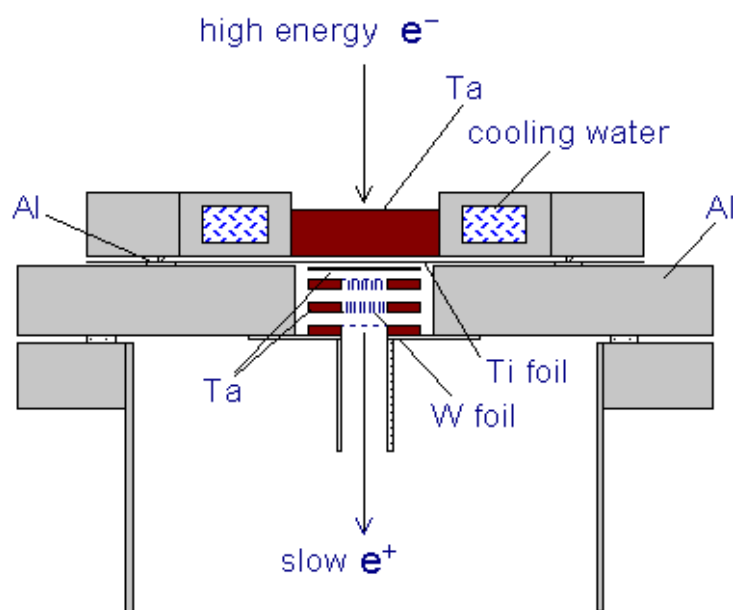


Figure 3. 1 Positron production and moderation in the positron beam at

AIST^[17]

These slow positrons are transported from the positron source to the experimental room by a magnetic transport system, as is shown in Fig. 3.2. The transportation distance, which is 20m long, can effectively reduce the background radiation. The magnetic field strength is about 7 mT in this transport system. The diameter of the beam when it passes through the transport system is more than 10 mm. The measured beam intensity is about $2-3 \times 10^7/s$.

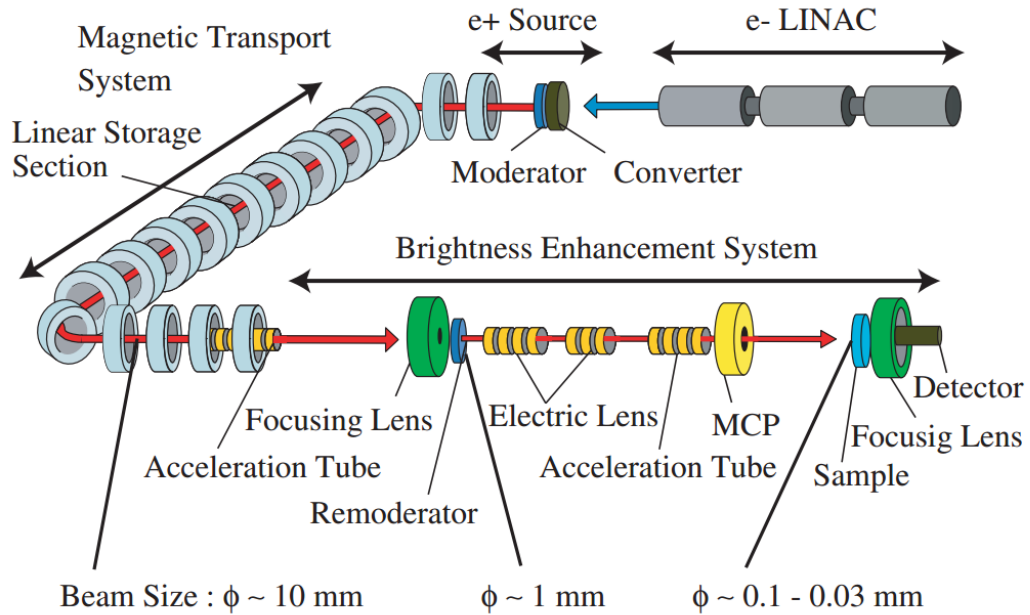


Figure 3. 2 Layout of the positron beam system at AIST^[18]

A brightness enhancement method is used to substantially reduce the size of beam spot at the expense of losing beam intensity. The beam is extracted from the magnetic field before it reaches the experimental room. The extracted beam is focused on a re-moderator by a lens to enhance its brightness. The re-moderator is a 200 nm thick single-crystal of tungsten. After re-moderation, the diameter of positron beam can be reduced to less than $30\mu\text{m}$ ^[19]. The efficiency of the transmission process in the re-moderator is about 5%. The beam intensity after the re-moderation is about $10^6/\text{s}$ ^[18].

With the slow positron micro-beam, three-dimensional imaging of defect distributions can be observed by the scan of $50 \times 50 \mu\text{m}^2$ in each step as shown in Fig.

3.3.

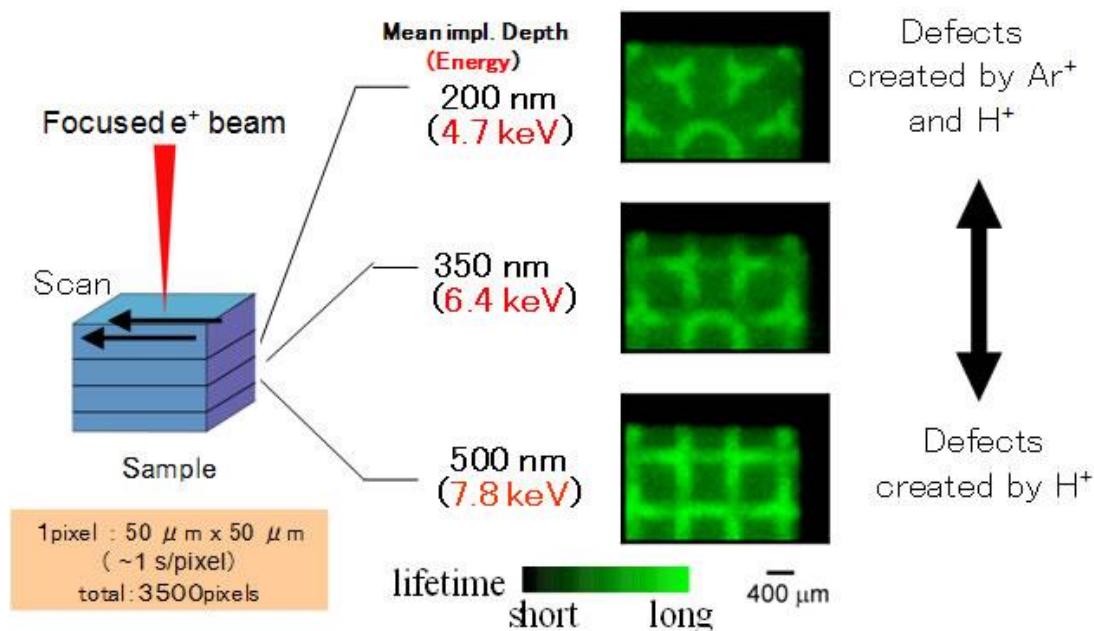


Figure 3. 3 PALS result using a Positron Probe Microanalyzer^[20]

3.1.2 Linac-based positron beams in other countries

The slow positron beam in the Institute of High Energy Physics (IHEP) in China was constructed in 2004, based on a 1.3 GeV linac^[21]. A Ta target is applied as the converter and a multi-layered tungsten mesh is used as the moderator for the beam, which are the same with the beam in AIST. The intensity of the beam is about $1.8 \times 10^5/\text{s}$. In pulse mode, an intensity of $6.5 \times 10^5/\text{s}$ can be achieved^[22]. The system is equipped with several measurement systems including slow positron annihilation lifetime spectroscopy (SPALS), coincidence

Doppler broadening spectroscopy (CDBS) and positron annihilation age-momentum correlation spectroscopy (AMOC).

Argonne positron source (APosS) is based on the linac in Argonne National Laboratory in United States. The linac is able to provide electrons with energy up to 20MeV. The converter of the beam was a piece of water-cooled tungsten. A tungsten foil was utilized in the system as the moderator. The demonstrated slow positron beam intensity was $3 \times 10^7/\text{s}$ ^[23]. An upgrade aimed at increase the beam intensity is ongoing. The upgrade includes increasing the efficiency of moderator, decelerating the fast positrons and increasing the accelerator beam energy.^[24]

ELBE Positron Source (EPOS) is a running project based on the superconducting linac in Rossendorf, Germany. The EPOS was designed for material research. Tungsten foils were applied as converter and moderator.^[25] A positron lifetime spectroscopy system is under construction to take advantage of the superconducting linac.^[26]

A new slow positron beam based on a compact, low energy (4.3MeV) linac recently has been constructed in Saclay, France. The primary aim for the beam is to produce positrons for the GBAR experiment (Gravitational Behavior of Antimatter in Rest) approved by CERN.^[27] The development of the beam also towards the aim to commercialize the compact non-radioactive slow positron source for materials research. The beam is currently operated with a tungsten converter and a tungsten moderator. A positron beam flux of $2 \times 10^6/\text{s}$ has been achieved.^[28]

3.2 Reactor based positron beams

To achieve even higher count rates, reactor based positron sources have been developed, although there are only a few such sources in the world. The major difference of the principle between the linac-based positron beam and nuclear reactor based positron beam is that, in linacs-based beams, the γ rays are produced by the bremsstrahlung of high energy electrons. However, in the nuclear reactor based beams, the gamma rays are produced by nuclear reaction. The gamma rays produced by the fission reactions in the core of reactors can be used. A more effective setup of a reactor based positron source is based on the principle of thermal neutron capture by cadmium. This process is mainly based on the nuclear reaction $^{113}\text{Cd} (n, \gamma) ^{114}\text{Cd}$ due to the very large cross section of ^{113}Cd for thermal neutron capture (of the order of 20,000 barn at 0.0253 eV)^[29]. The effective cadmium thermal neutron capture cross section is only 2,500 barn because the abundance of ^{113}Cd is 12.22% in natural cadmium. The neutron binding energy of 9.041 MeV is released as gamma radiation, which can produce 3.6 gamma rays in average with energies of more than 1.5 MeV. The high energy gamma rays ($E > 1.022$ MeV) generated can then be converted to electron–positron pairs from a (γ, pair) nuclear reaction. The energy of the positrons produced in this way depends on the energy spectrum of the produced gamma radiation (approximately 1 MeV for a Cd-based source, the average energy of emitted gamma rays is 2.3MeV). The gamma-pair

conversion should take place in the material with a high nuclear charge Z , since the cross-section for pair production is approximately proportional to Z^2 ^[30]. Therefore, metals with a high density are suitable to be used as converters. For high-energy photons, pair production is the dominant interaction process. However, at low energies (below 10 MeV), the Compton scattering and photoelectric absorption can become significant.

3.2.1 POSH

POSH, is an intense slow positron beam based on the 2MW Delft Research Reactor at Delft, Netherlands. The beam is equipped with 2-dimensional angular correlation of annihilation radiation (2D-ACAR) and Doppler broadening measurement systems, mainly used for material characteristic. The beam became operational in the year 2000 and it was the first available reactor based positron beam in the world. As a pioneer, Van Veen et al. tried different settings for the sources. At the beginning, they used copper activation to provide positrons^[31]. Then they modified the design and used tungsten to produce positrons by pair production from gamma radiation near the reactor cores^{[32][33]}. As is shown in Fig. 3.4, three disks R1, R2, and R3, which are covered by tungsten, generate the positrons by pair

production. Fast positrons are moderated by tungsten cylinders in the disks and emitted from the internal tungsten surfaces.

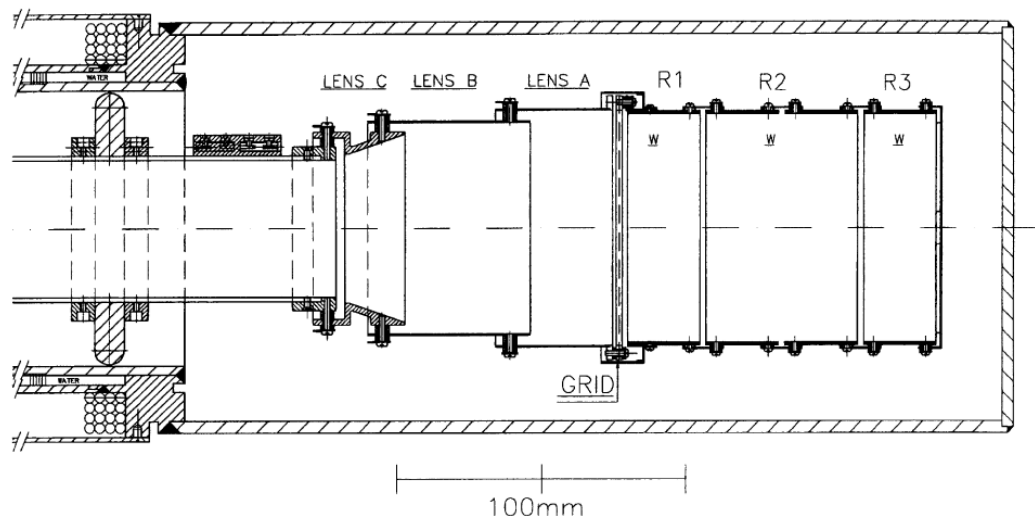


Figure 3. 4 The 1997 configuration of the positron source of POSH. [32]

Positrons were observed with an intensity of nearly $10^8/s$ in a 3.3 mm (FWHM) beam spot. Beam transport efficiency over a 25m distance is about 95%. After 3 years running, the long term performance of the source was examined. As shown in Fig. 3.5, the intensity of the beam had decreased from $2 \times 10^8/s$ to $10^8/s$ after one year's operation.

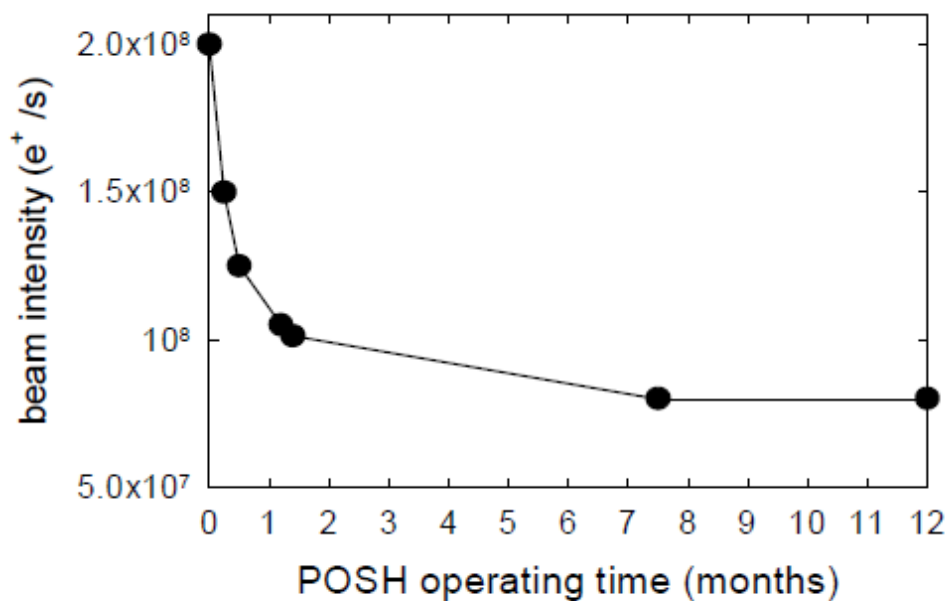


Figure 3. 5 Decrease of beam intensity with time^[34]

The radiation damage of the tungsten may be one of the reasons to explain the decrease of the beam intensity. A clear increase of the S parameter of the tungsten foil is observed after long term irradiation by neutrons (as shown in Fig. 3.6), indicating that a large number of defects were created during the irradiation time.

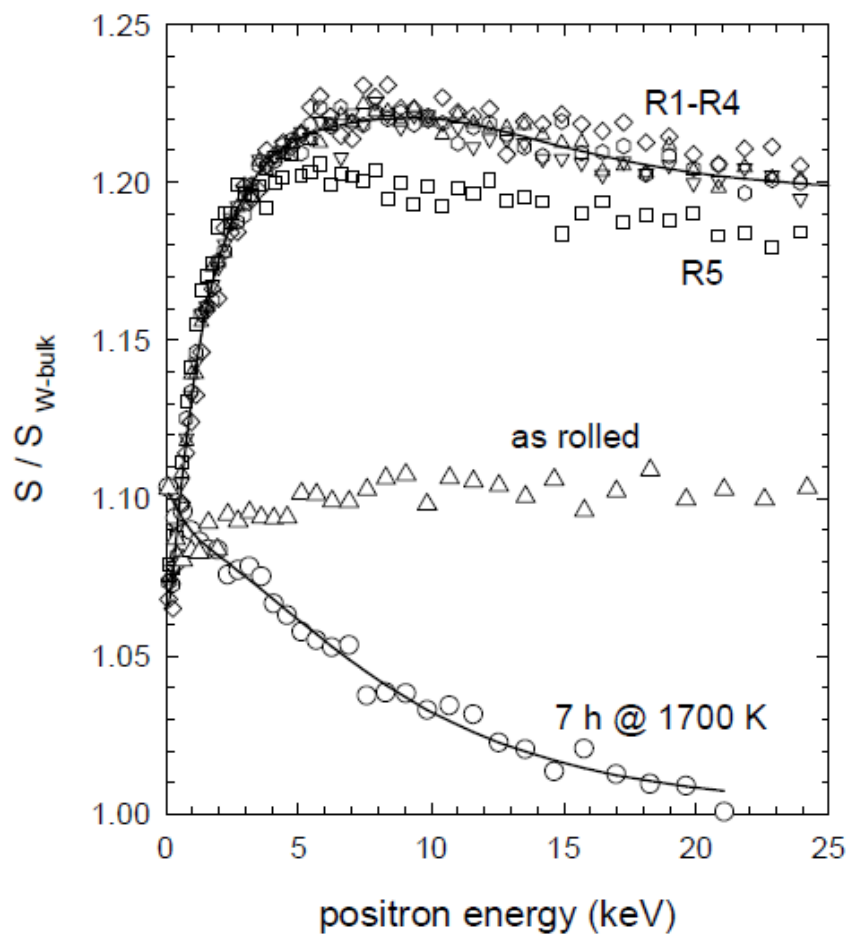


Figure 3. 6 S parameter of tungsten foils. The data are shown for tungsten foils: used in the POSH source for 3 years (R1-R5); as rolled; annealed for 7 hours at 1700K in vacuum.^[34]

3.2.2 NEPOMUC

The NEutron induced POSitron source MUniCh (NEPOMUC) in Germany is a positron source based on a 20 MW research reactor^[35]. Positrons are generated by pair production of high energy gamma rays from neutron capture in cadmium. The

positron beam was first observed in 2002^[36] and the first experiment was launched in 2006. After more than 5 years running, the facility was upgraded in 2012^[37]. After the upgrade process, the old source tube was replaced by a new one using 80% ¹¹³Cd enriched Cd, which would extend the operation time to 25 years. A tungsten re-moderator was installed in the system aimed to increase the brightness of the beam. Until now, the beam line has been equipped with the measurement systems including pulsed low energy positron beam system (PLEPS), coincidence Doppler broadening spectroscopy (CDBS), positron annihilation induced Auger electron spectroscopy (PAES)^[38].

The structure of the whole positron source includes three main components: the outer beam tube containing the Cd converter inside the tip, the inner ‘experimental tube’ that carries the magnetic coils for positron beam transport, and the innermost ‘potential tube’ with the Pt foil structure and electric lenses for beam extraction. A cross-sectional view of the positron source inside the beam tube tip is shown in Figure 3.7.

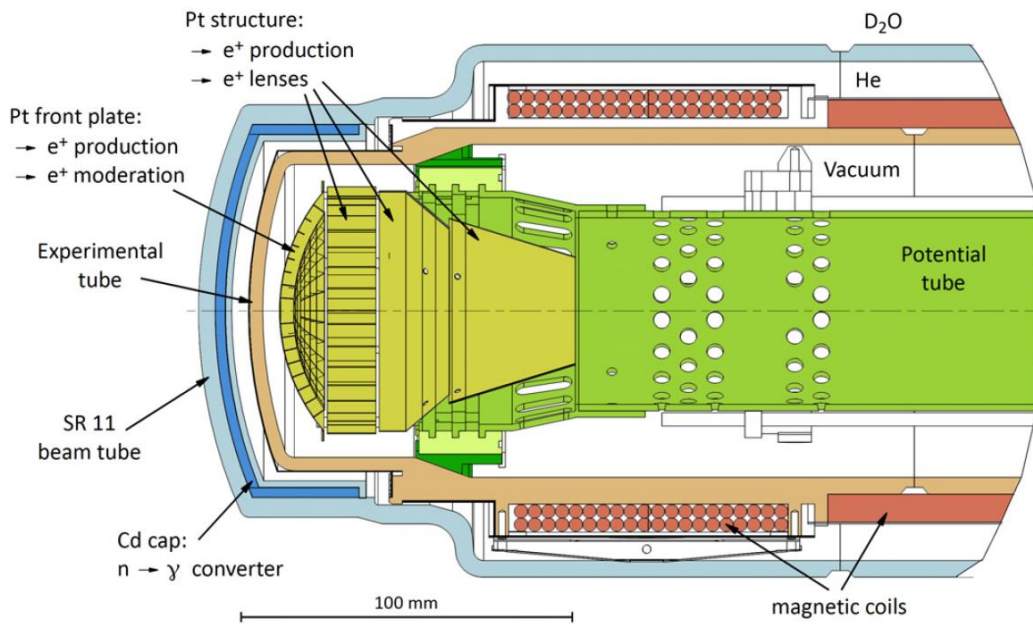


Figure 3. 7 Structure of the positron source tube in NEPOMUC^[37]

A structure of Pt foils is used for positron production since the cross-section of pair production using Pt is about 11% higher than that using W at other sources. Compared with W, Pt has an additional advantage of a lower annealing temperature, which is easier for the *in situ* annealing to reduce the irradiation-induced vacancies.

3.2.3 PULSTAR

PULSTAR is a 1-MW reactor based source located at North Carolina State University in United States. It is the third reactor based positron beam in the world and the first one in North America. The PULSTAR reactor is a swimming pool type research reactor. The light water surrounding the core acts as both a neutron

moderator and a coolant. The reactor core is designed in a highly under-moderated way which allows the thermal neutron flux to peak at the core edges near the entrance of the beam tube. In this way, the intensities of neutrons and gamma rays can be comparable to those from the reactors with higher power.^[39]

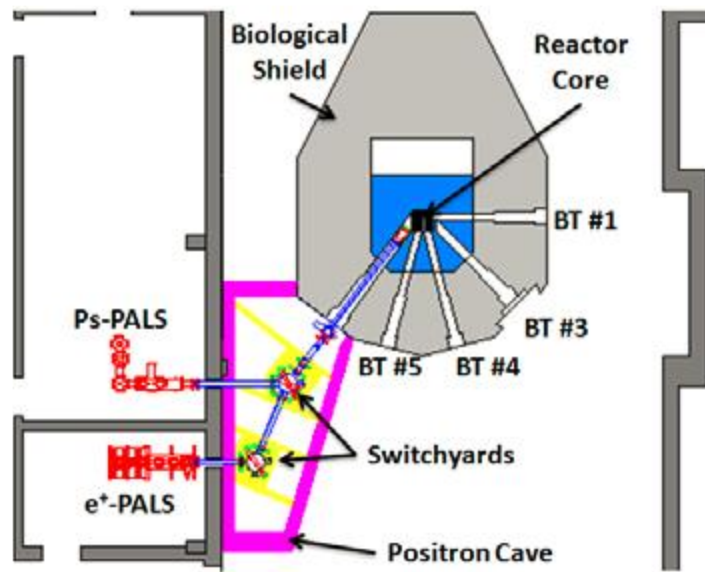


Figure 3. 8 The layout of the slow positron beam in PALSTAR reactor^[39]

The positron beam is launched on one of the five beam ports in the reactor, as is shown in Fig. 3.8. The beam is operated with an intensity of approximately 5×10^8 e⁺/s^[40]. The positrons are generated through gamma ray pair production interactions in two back-to-back banks of tungsten converter/moderators. The gamma rays are produced in the PULSTAR core and by thermal neutron capture in a cadmium shroud that surrounds the tungsten. The primary utilization of the PULSTAR positron beam is the characterization of nanoscale structures in materials.

The beam has been equipped with two PALS systems. The first is dedicated to measurements in materials such as metals and semiconductors. This spectroscopy is based on pulsing and bunching of the primary beam and is currently operating with a time resolution of approximately 390 picoseconds. The second is dedicated to measurements in materials where positronium formation is promoted. The time resolution of this system is designed to be ~0.5 nanoseconds with an on-sample spot size of 1-2 mm². For both systems, the energy of the positrons can be varied to allow depth profiling with on-sample intensity exceeding 10⁶ e+/s.

3.2.4 KUR and HIPOS

There are two other reactor based positron beams under construction. HIPOS is a launched Exploratory Research Project to design a very high intensity positron beam based on the High Flux Reactor (HFR) in Petten, The Netherlands. The HFR is a multi-purpose research reactor which uses light water as coolant and moderator^[41]. The nominal operating power is 45 MW. For the positron beam, tungsten was selected as the primary material for the generation of positrons as well as the moderator due to its already confirmed long-term stability. The other settings are similar to NEPOMUC as was shown in Fig. 3.9. Based on their calculations, fluxes of slow positrons of the order of 10¹⁰ e+/s can be expected.

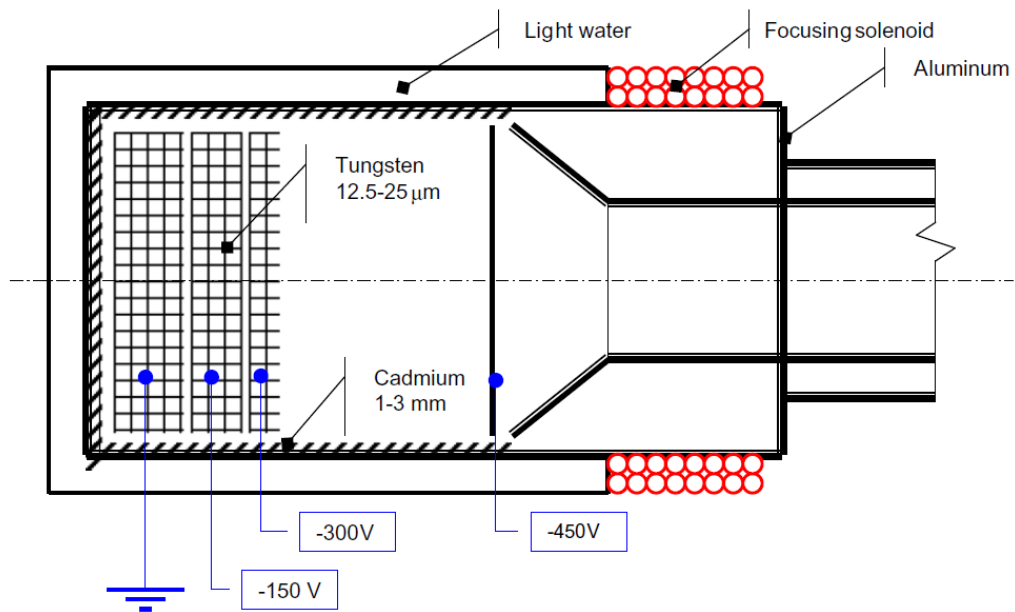


Figure 3. 9 Schematic drawing of HIPOS positron generator^[41]

The KUR is a light-water-moderated tank-type reactor located at Kyoto University in Japan operating at a maximum thermal power of 5 MW. The design of the positron beam also followed the concept of NEPOMUC. Tungsten is used as the converter and moderator. Currently, the intensity of the beam is $1.4 \times 10^6/s$ while the reactor is being operated at a reduced power of 1 MW and the diameter of the beam spot is about 2cm. The schematic of the positron beam line is shown in Fig. 3.10. Sato et al.^[42] are planning to add a beam bunching unit to convert the continuous beam to a pulsed beam. A brightness enhancement unit is also in development to decrease the size of beam and increase the brightness.

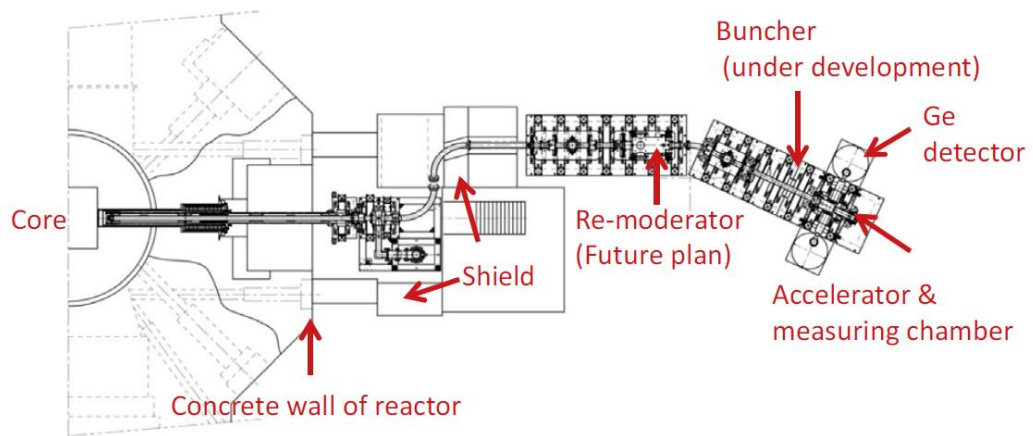


Figure 3. 10 Top view of the positron beam line and the material irradiation chamber at KUR^[42]

Chapter 4 – The McMaster Intense Positron Beam Facility (MIPBF) Project

4.1 MIPBF Overview

The McMaster Intense Positron Beam Facility (MIPBF) is a reactor-based positron beam facility that is to be installed on one of the beam ports of the McMaster Nuclear Reactor (MNR). The MIPBF is a collaborative project involving several McMaster researchers, MNR staff members, numerous external research partners and collaborators, as well as funding agencies such as the Canada Foundation for Innovation and the Ontario Ministry of Research & Innovation. When complete, the MIPBF will be the first reactor-based positron production facility in Canada. Initially, the facility will include two experimental stations: a Defect Characterization System for examining near-surface regions and thin films by techniques such as coincidence Doppler broadening and positron lifetime spectroscopy and a Positron Storage and Interaction System which will permit fundamental research into the nature of the interactions of antimatter, such as the formation of anti-hydrogen.

The McMaster Nuclear Reactor (MNR) is a light-water swimming-pool-type research reactor located on the campus of McMaster University in Hamilton,

	POSH	NEPOMUC	NCSU	MIPBF
Reactor Type	MTR-pool	Compact high flux	PULSTAR	MTR-type
Reactor Power	2 MW	20 MW	1 MW	3 MW
Reflector	H ₂ O	D ₂ O	H ₂ O	H ₂ O
Φ_{th} (/cm ² /s)	-	2×10^{14}	2.5×10^{12}	$6 \text{ to } 8 \times 10^{12}$
$\Phi_{th:qf}$	1 to 1.6	$>10^4$	NA	0.7 to 1.3
Source Generation	II	II	I	Design
Beam-tube geometry	Radial straight	Radial angled	Radial angled	Radial straight
Beam-tube OD	6"	3.5"	$> 8"$	8"
Target Material	Ti/W	Ti/Pt	W	Ti/Pt
Target Geometry	Grid	Plate & Sleeve	Grid	Plate & Sleeve
Target OD	3.1" (8cm)	2.6" (6.5cm)	9" (23cm)	7" (17.8cm)
Target foil thickness	0.25 mm	0.15 mm	0.25 mm	0.15 mm
Cd Converter	No	Yes	Yes	Yes
Cd thickness	-	3 mm	0.2 mm	1mm
Primary slow e ⁺ /s	4×10^8	1×10^{10}	$\sim 7 \times 10^8$	Target $\sim 1 \times 10^9$
Remoderated e ⁺ /s	-	9×10^8	-	-

Table 4. 1 Comparison of the parameters of four reactor based positron beams^[43]

The model of the source tube of MIPBF is shown in Fig. 4.2. The source tube is supported by an aluminum beam-tube liner. A cadmium end cap with a thickness of 1mm is mounted on the aluminum beam-tube liner to provide additional γ rays. A vacuum tube is inside the aluminum liner. A titanium faceplate (18cm diameter, 7mm thick) covered by a platinum foil (0.15mm thick) is placed in the vacuum tube. A platinum sleeve (18cm diameter, 0.15mm thick) extends for a distance of 10cm down the beam tube to convert the γ rays from the sides of the tube. Platinum was selected as the material of converter because it has some advantages compared with tungsten. Firstly, platinum has larger pair-production cross section

(15-20% over a 2-7 MeV range) than tungsten. Secondly, the annealing temperature of platinum (700-800K) is apparently lower than that of tungsten (1700K). Additionally, platinum has the potential to resist the degradation caused by the neutron irradiation.^[43]

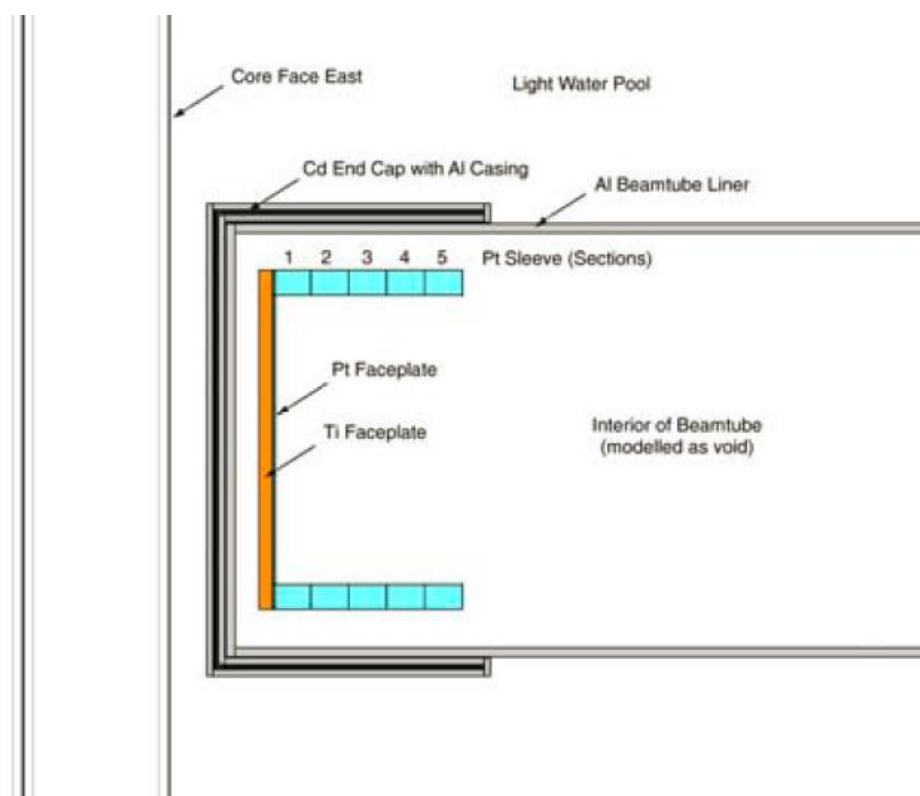


Figure 4. 2 Model of the positron source tube at MNR^[43]

Two teams are working on the various components of the MIPBF. One is developing the positron source in the reactor, including the conversion of the gamma rays, moderation of positrons and extraction of slow positrons. The other is developing the defects characterization system, which will be described in Chapter

4.3. When the installation of the source part in the reactor is completed, the characterization system will be moved into the reactor area and connected with the source.

The defect characterization system consists of two parts: the measurement system, and the spectrum acquisition and analysis system. The measurement system was designed and manufactured by CAP Engineering Co. in France. The spectrum acquisition and analysis system was purchased from Ortec. Then the systems were delivered to Western University in London, Ontario for out of core test. Before the delivery, the original positron beam system at Western University was separated into two parts. The sample chamber of the original beam system was removed and the source chamber was left to provide a test positron beam for the new characterization system. Then, the original source part and new characterization system were assembled and installed together as a new positron beam system. In this way, the new defect characterization system can be tested.

4.2 Spectrum acquisition and analysis system

The defect characterization system was designed to enable both coincidence Doppler broadening spectroscopy (CDBS) and positron lifetime measurements. For the former, the spectrum acquisition and analysis system focuses on gamma ray

energy spectroscopy. All the components in the system were purchased from Ortec, including two high-purity Ge detectors, two 579 fast filters, two 583B Constant Fraction Differential Discriminators (CFDD), a 414A Fast Coincidence, a 416A Gate and Delay, one digital gamma spectrometer DSPEC 502 and delay boxes.

The output signals from the detectors are pulses with positive voltage. However, the input of 583B CFDD needs to be negative. Therefore, a 579 fast filter amplifier is connected between the detector and the CFDD to reverse and amplify the signal. The CFDD is to provide timing signal for coincidence. Users can adjust the shaping delay of the CFDD by applying a delay between a pair of front-panel DELAY connectors on the CFDD. The delay box for the CFDD was designed to be DB463. Alternative to the DB463 is two 425A Delay modules. The signals (positive logic signals) produced by two CFDDs are input into the 414A Fast Coincidence. The coincidence output signals from 414A then can be imported into 416A Gate and Delay. The 416A can convert the coincidence signals to gate signals and adjust the delay of the gates. The 416A is connected to the Gate Input connector on the rear-panel of DSPEC 502 to provide gate signals. The DSPEC 502, which is a landmark product of Ortec, is a digital gamma spectrometer especially designed for HPGe detectors. The DSPEC 502 is a combination of two separate MCAs and a digital spectrum stabilizer, equipped with advanced Digital Signal Processing (DSP)

algorithms, which can produce an enhanced spectroscopic performance. To realize the coincidence, the components will be connected as shown in Fig. 4.3

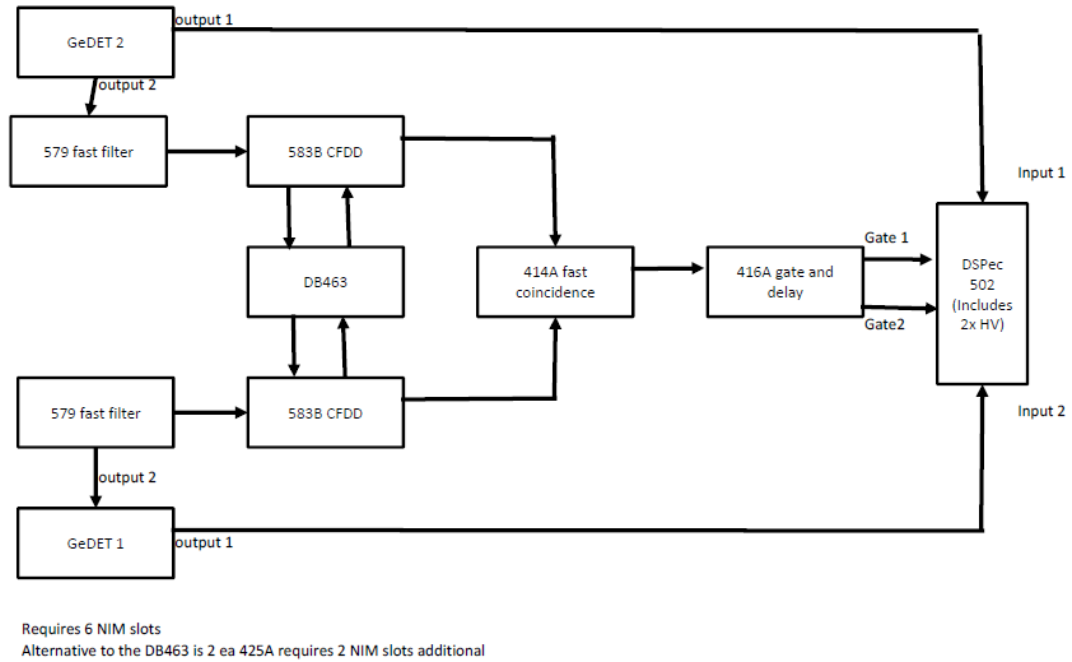


Figure 4. 3 Schematic of the CDBS set-up

4.2.1 Detector performance test

As the first step, the detectors' properties need to be tested to ensure that they meet the standard level. In this test, a $1 \mu\text{Ci } ^{22}\text{Na}$ and a $1 \mu\text{Ci } ^{137}\text{Cs}$ sealed source were used. The software used to collect the gamma ray spectra is called MAESTRO (as shown in Fig. 4.4), purchased from Ortec. The MAESTRO software is the most widely used software that can collect positron Doppler broadening as well as positron annihilation lifetime spectra. When the software is applied to collect

Doppler broadening spectra, each channel corresponds to an energy. Before the first use of the software, it needs to be calibrated by a radionuclide, which has at least two peaks in the energy spectrum. In our experiment, the software was calibrated using ^{22}Na before testing the detectors.

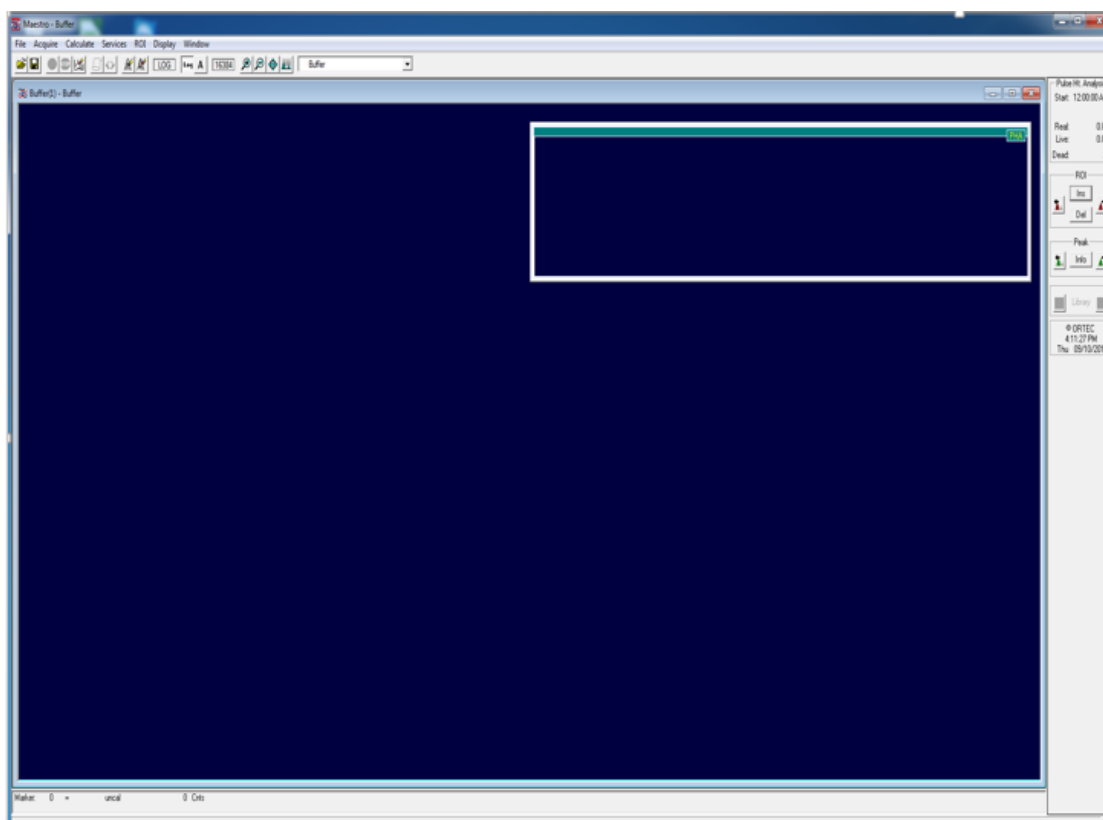


Figure 4. 4 User interface of MAESTRO

The energy resolution of HPGe detectors is much better than that of other kinds of detectors, such as NaI. The nominal energy resolutions (FWHM) of our detectors as per the manual are listed in Table 4.2:

**Table 4. 2 Energy resolution of HPGe detectors measured with a Co-60 source
at the 1.33MeV peak**

Detector	Best performance voltage	Energy resolution
1	3200V	1.65keV
2	4800V	1.85keV

For Detector 1, the ²²Na energy spectrum is shown in Fig. 4.5. The FWHM at 511keV is 2.41eV and at 1274keV it is 1.62eV.

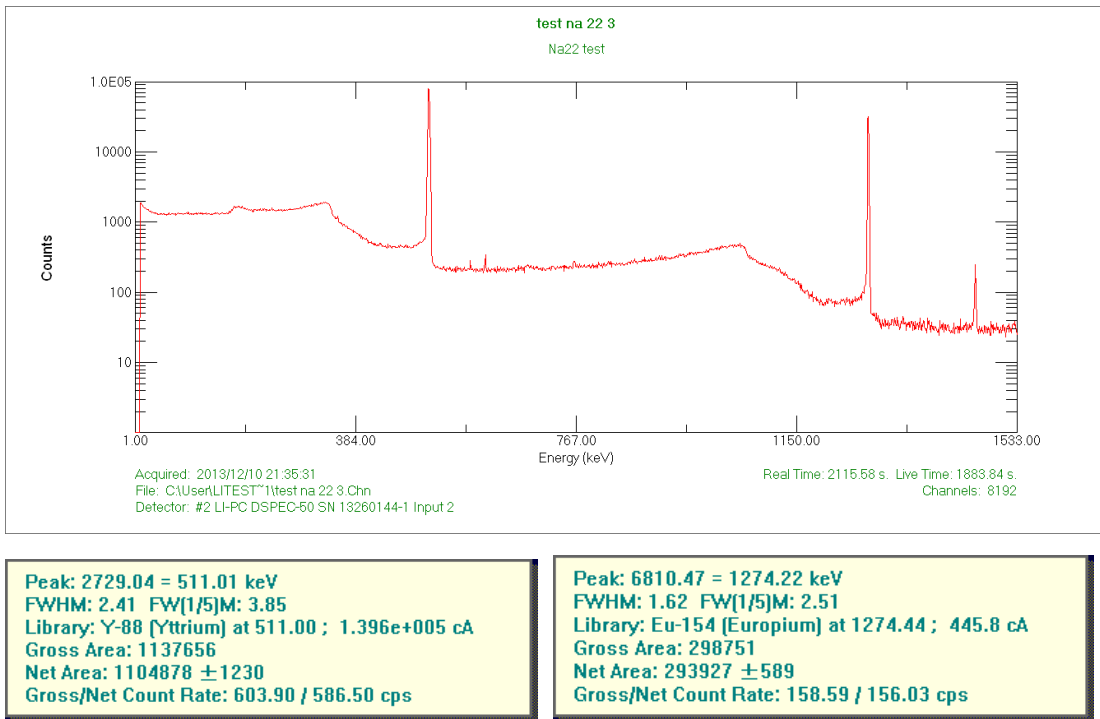


Figure 4. 5 ²²Na energy spectrum from Detector 1

For Detector 2, the ^{22}Na energy spectrum is shown in Fig. 4.6. The FWHM at 511keV is 2.48eV and at 1274keV it is 1.90eV.

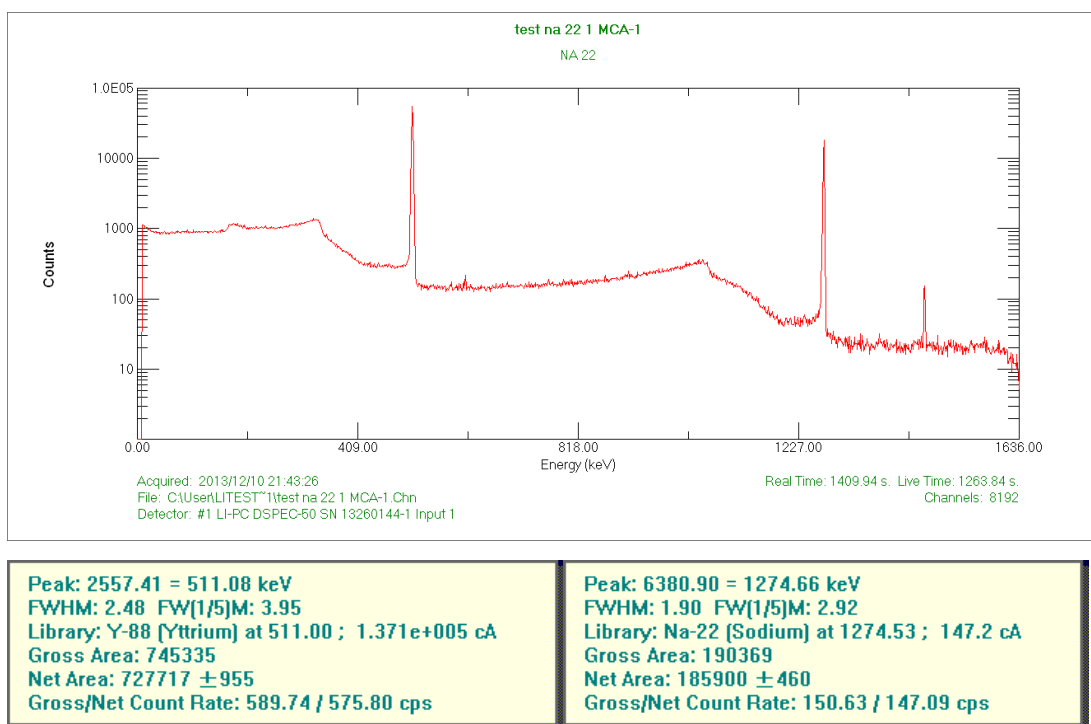


Figure 4. 6 ^{22}Na energy spectrum from Detector 2

For Detector 1, the ^{137}Cs energy spectrum is shown in Fig. 4.7. The FWHM at 661keV is 1.24eV and at 1460keV it is 1.68eV.

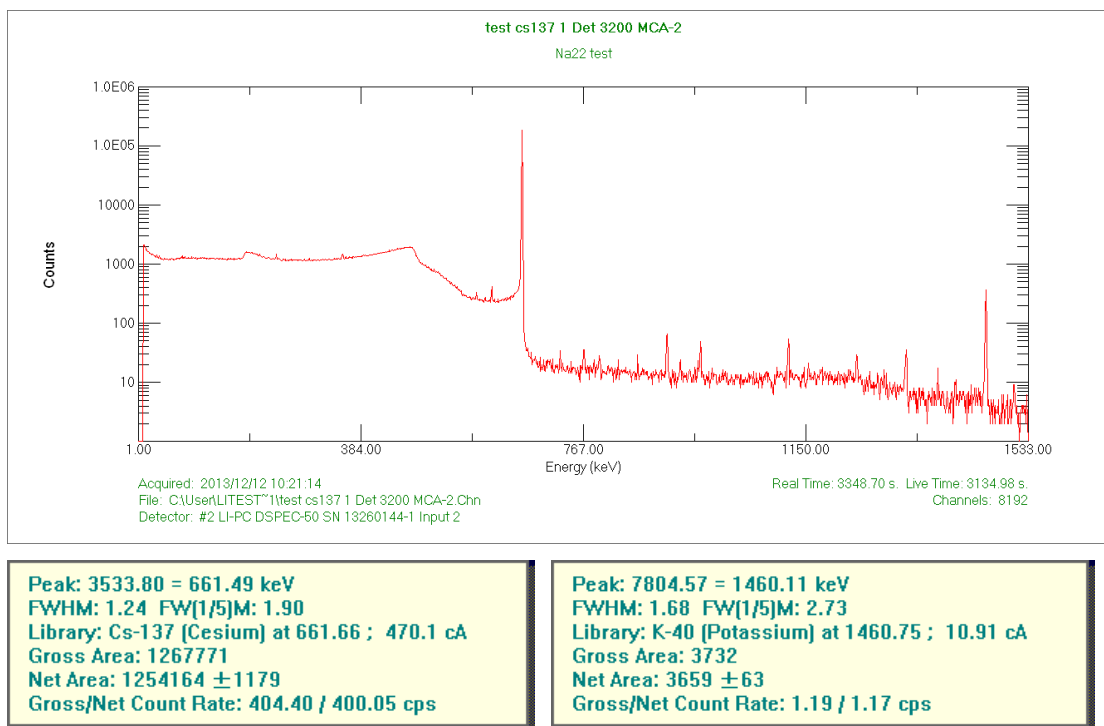


Figure 4. 7 ¹³⁷Cs energy spectrum from Detector 1

For Detector 2, the ¹³⁷Cs energy spectrum is shown in Fig. 4.8. The FWHM at 661keV is 1.36eV and at 1460keV it is 1.93eV.

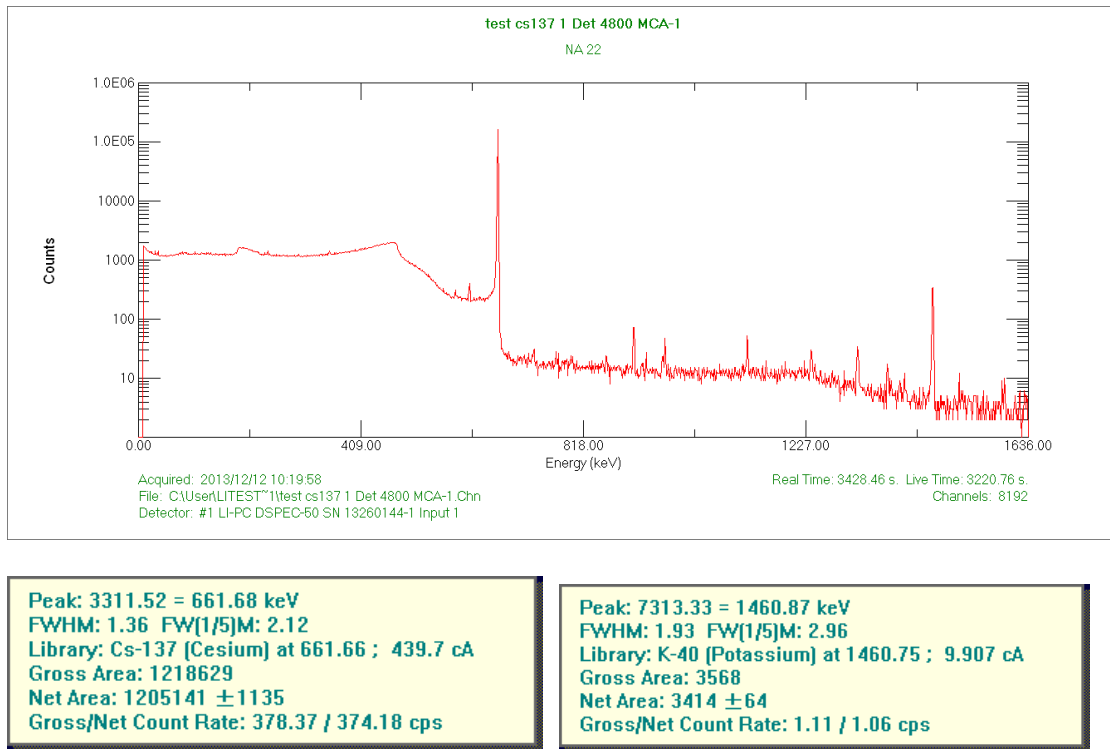


Figure 4. 8 ^{137}Cs energy spectrum from Detector 2

With the same ^{137}Cs source, the count rate was increased from $\sim 1500/\text{s}$ to $\sim 2300/\text{s}$ and the collecting time was increased as well. The resulting energy resolution is shown in Figs. 4.9 and 4.10. By increasing the count rate and gross counts, the energy resolution became better because the signal to noise ratio is increased. By comparing the results with the standard energy resolution on the manual, it can be concluded that the quality of detectors meets the standard.

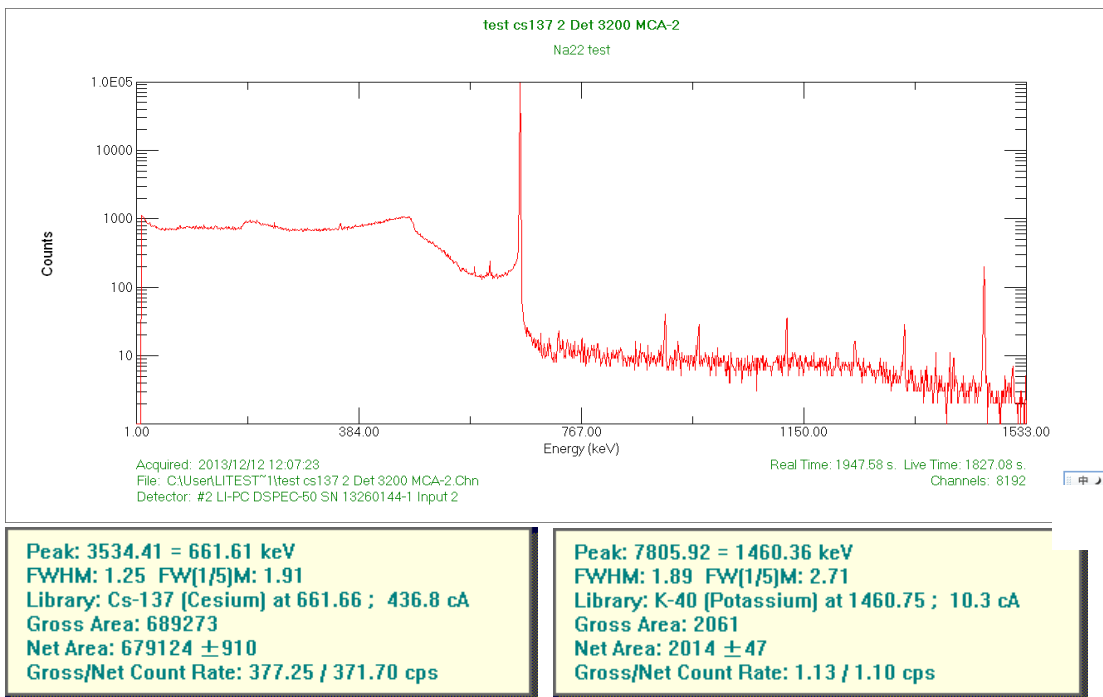


Figure 4. 9 ¹³⁷Cs energy spectrum from detector 1 with more counts

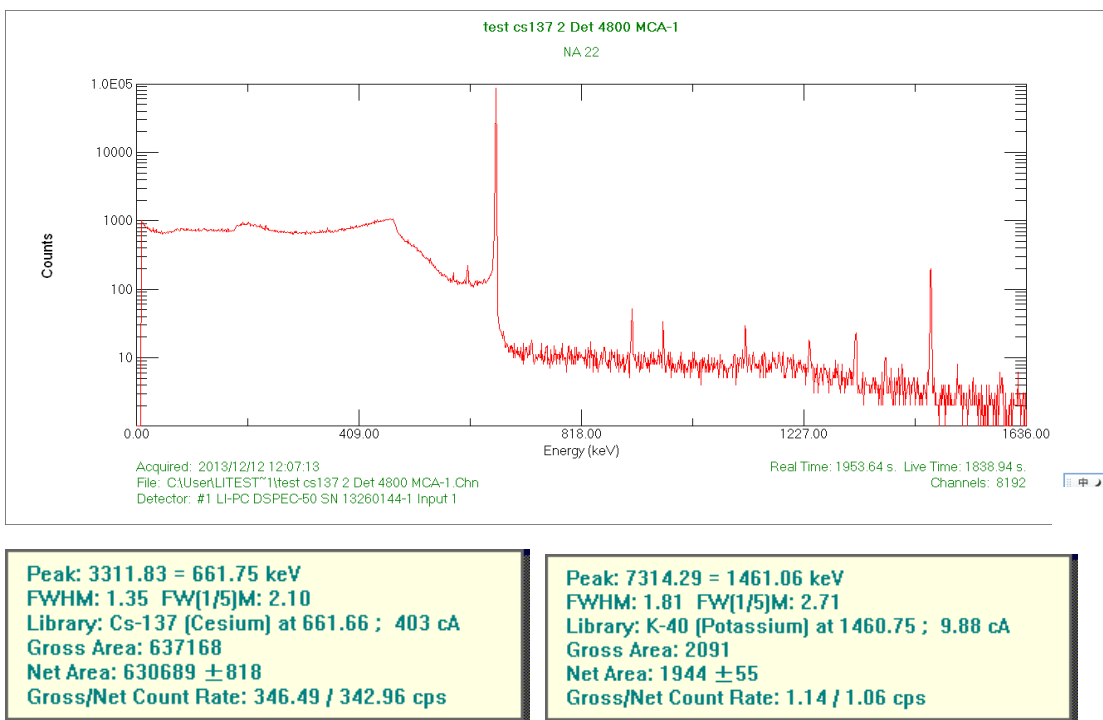


Figure 4. 10 ¹³⁷Cs energy spectrum from Detector 2 with more counts

4.2.2 Coincidence setting

The steps to set the coincidence are as follows (the detailed procedure will be provided later in this chapter):

1. Examine the output signals of the components in the system. Refer to the manual of each component to make sure that the signals from detectors, 579 Amplifiers, and CFDDs are reasonable, including polarity and scale.
2. Correspond the scales on the CFDDs to energies. Set the upper and lower levels of the two CFDDs to define the energy window of $511 \pm 50 \text{keV}$.
3. Input the signals from the CFDDs into the 414A Fast Coincidence. Convert the output signal of the Fast Coincidence to gate signal by 416A Gate and Delay.
4. Input the gate signal and another output signal from the detector into the DSPEC 502 (MCA) to get the coincidence energy spectra.

The operational principle of the 583B discriminator (as shown in Fig. 4.11) is to attenuate the input signal, invert, delay, and overlap it with the original signal in order to set the start point to count the event. The Constant Fraction (CF) delay thus needs to be calculated first. The length of CF delay depends on the charge collecting time of the detector. Based on the operational manual of our HPGe detectors, the CF delay of 583B is around 35ns. As reference, the delays of standard cables are:

Delay for RG 62A/U cable 3.92736ns/m

Delay for RG 58A/U cable 5.05274ns/m

Due to the fact that cables long enough to delay the signals were not available, delay boxes are needed.

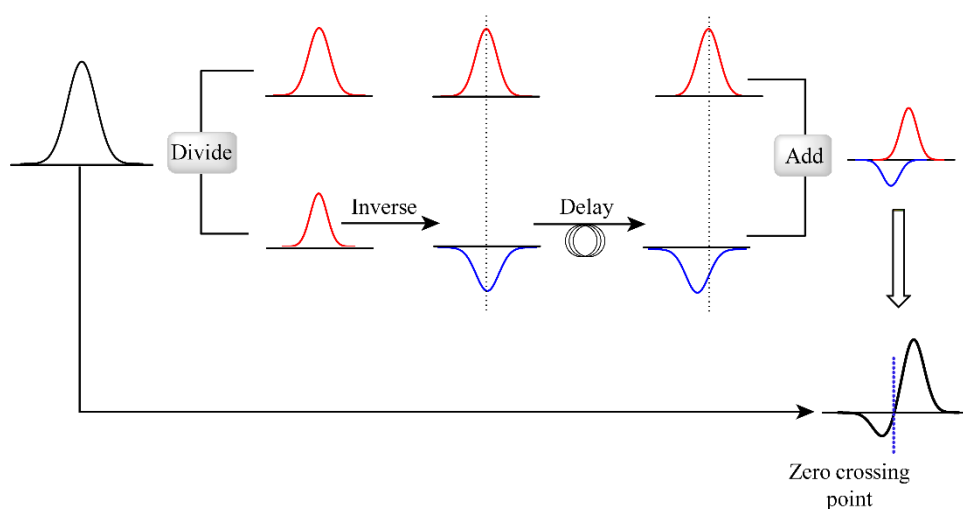


Figure 4. 11 Operational principle of a CFDD

After connecting the CF delay, the voltage scale on the CFDD needs to correspond to the γ -ray energy. There are two ways to accomplish this task. One is to set the window on the CFDD by adjusting the upper and lower levels. The next step is to record the count rate in each window and plot the result. By comparing the result with the known energy spectrum of ^{22}Na , the peak position can be located.

For the detector, based on the manual, signal output is 175mV/MeV. As for the 511keV and 1.027MeV peaks of ^{22}Na , the signals from the detector are around

positive 100mV and 200mV (measured on an oscilloscope), respectively. The signals from the detectors then be delivered to 579 fast filter amplifier. The 579 fast filter amplifier can reverse the polarity of the signals and amplify the signals. The output signals of the amplifier for 511keV and 1.027MeV peaks can be respectively set to about -2V/-4V on an oscilloscope, by adjusting the gain on the front-panel of the amplifier. The CFDD accepts negative pulses from 0 to -10V. The discriminator on the front-panel of CFDD ranges from -0.03V to -5V. To do the measurement, the upper level of the discriminator was fixed at 5V, and the lower level was adjusted from 5V step by step towards 0. The output of CFDD was connected to a counter. The count rate was recorded three times for each step to get the average. For the series of average numbers, a data processing procedure using $A_{n+1}-A_n$ to get the count rate for each step is shown in Appendix A. Then the plot of $(A_{n+1}-A_n)$ vs. lower limit voltage is shown in Fig. 4.12. From the figure, one can see that a peak occurs around 1.6V.

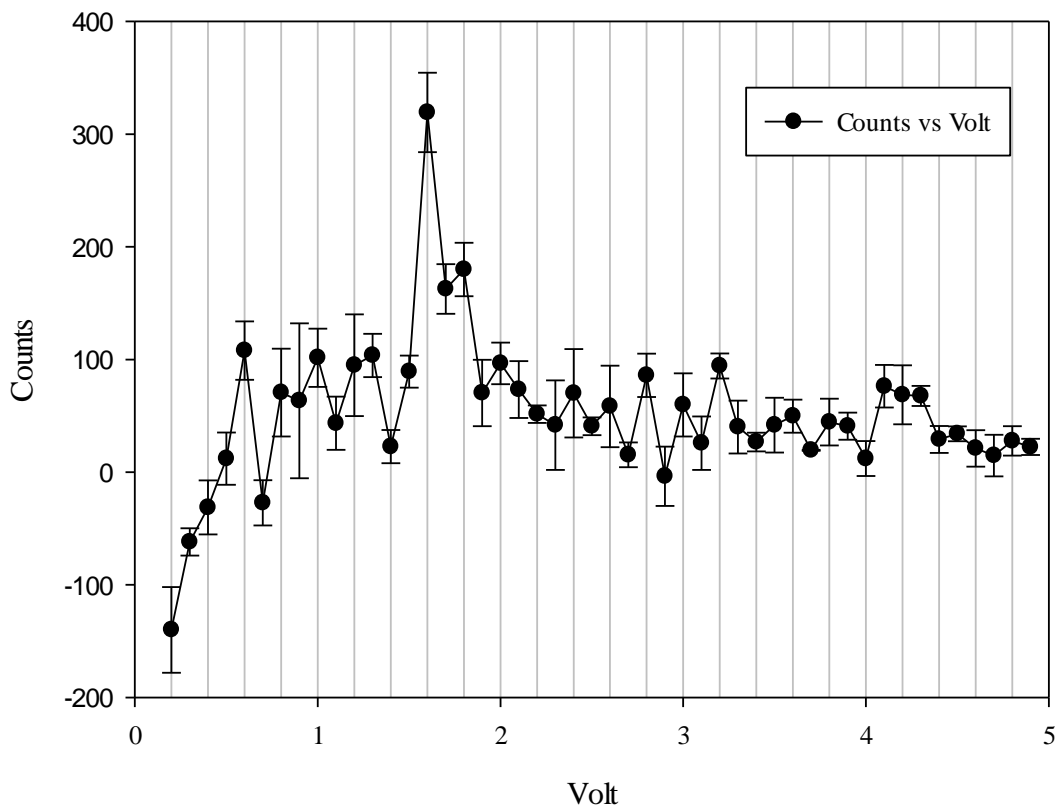


Figure 4. 12 Energy spectrum based on the voltage range on discriminator

Another way to correspond the scale on the discriminator with energy is to directly observe the region between the energy window in MESTRO software. To use this method, a simple coincidence system needs to be connected as is shown in Figure 4.13.

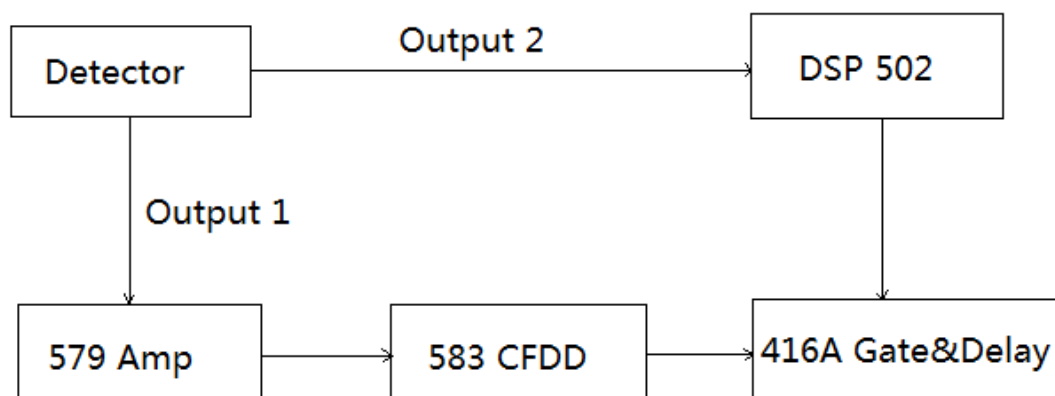


Figure 4. 13 Single detector coincidence

The principle of this method is to use the coincidence of the same event signal from two outputs. The signal from output 1 is a full energy spectrum, and the signal from output 2 will be cut by the energy window of the CFDD and work as a gate. If the signal from output 1 arrives at the DSP 502 at the same time with the gate signal, the spectrum in MESTRO will range only in the region between the upper level and the lower level. The next step is to adjust the delay to ensure that the signal from output 1 can get into the gate. In order to have a clearer view of the spectrum, it is better to set the width of the gate at maximum $4\ \mu\text{s}$.

A randomly collected spectrum with a large energy window between 0.5V-3V is shown in Fig. 4.14

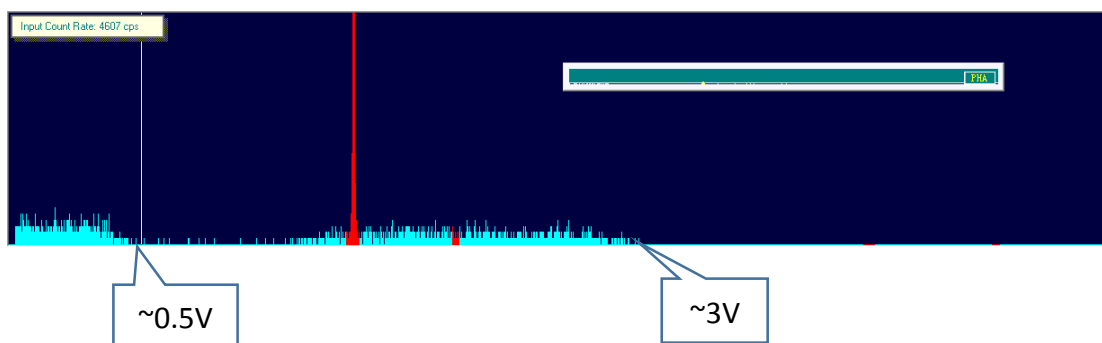


Figure 4.14 Randomly collected spectrum

By comparing Fig. 4.14 with the ^{22}Na energy spectrum in Fig. 4.6, it is obvious that the red peak is the 511keV peak, and it locates at a position around 1.6V. However, the distribution of the counts in other regions is not similar to the ^{22}Na energy spectrum, which means the delay value is not right. Then a region around 1.6V such as 0.3V-1.8V was selected and the delay was adjusted as in Fig. 4.15.

From Figure 4.15, it is seen that a reasonable delay is between $1\ \mu\text{s}$ and $3\ \mu\text{s}$, because the shape of spectra at these delay times are similar to the ^{22}Na energy spectrum. In the next step, the energy window on the discriminator can be narrowed down to 1.5V-1.8V in order to correspond to the energy of γ rays precisely.

(1) 0.3V-1.8V; delay 1us. 511keV Peak FWHM 2.18. Counts 3165



(2) 0.3V-1.8V; delay 2us. 511keV Peak FWHM 2.36. Counts 3722



(3) 0.3V-1.8V; delay 3us. 511keV Peak FWHM 2.35. Counts 3832



(4) Detector 2 - 0.3-1.8V; delay 4us.



Figure 4. 15 (1)(2)(3)(4) are coincidence spectra with delays from 1 to 4 μs

Comparing the results in these two ways to correspond the scale on the discriminator with the γ energy, it is easy to get the same result that the 511keV peak is around 1.6V. Additionally, from the second method, background signals from the γ rays with the energy lower or higher than the selected energy range can be cut off. In this way, a simple coincidence spectrum with a better signal-to-noise ratio (SNR) can be obtained. After each coincidence step, the SNR will increase while the count rate will decrease, which means that the time to take the measurement will increase. The original setting of the system includes two pairs of coincidence, which will significantly decrease the count rate and increase the time to measure samples.

4.3 Positron beam system

4.3.1 Overview

The positron beam line is now being tested out of core at Western University in London, Ontario, Canada (an image is shown in Fig. 4.16). The source chamber was part of the positron beam system constructed in the 1990s (an image is shown in Fig.4.17). The new defect characterization system (an image is shown in Fig. 4.18) was shipped from France and assembled in Canada in May, 2014.



Figure 4. 16 The current positron beam facility at Western University

The original positron beam system was designed for positrons to be accelerated solely from the source chamber. This means that the source chamber was on high voltage. As a result, the source part needed to be isolated and operated by a control system. In the new positron beam system, positrons are accelerated by the high voltage at the sample chamber. Therefore, the source part can be operated manually. However, attention still needs to be paid to avoid electric shock as a voltage of several hundred may occur.

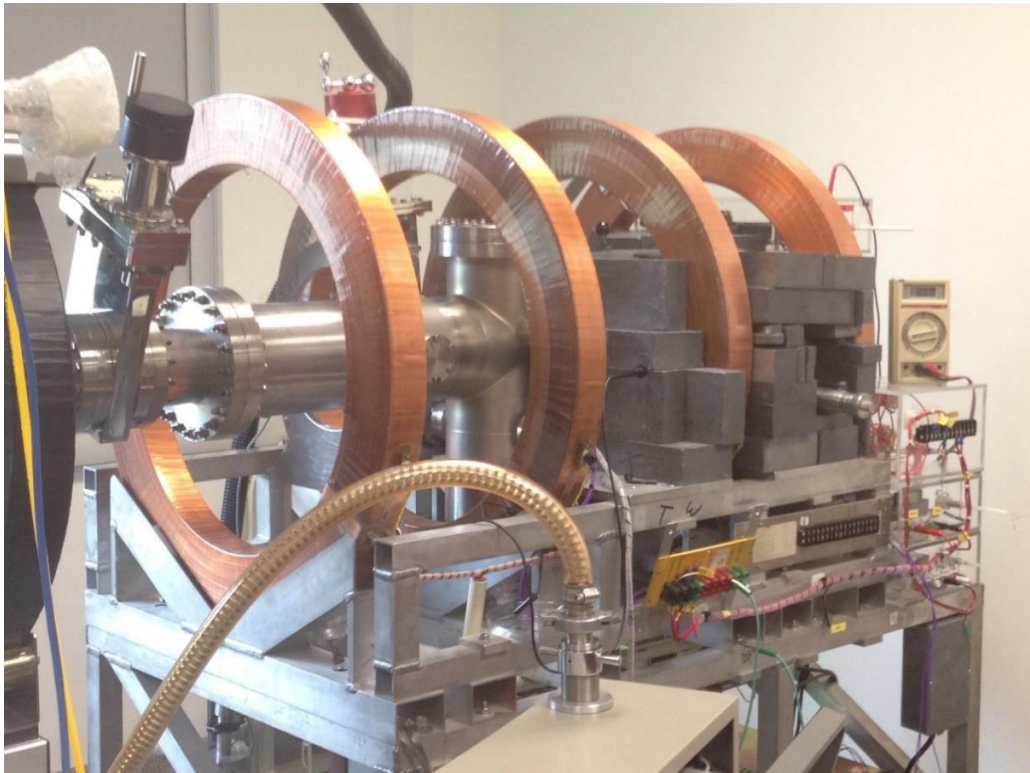


Figure 4. 17 Original source chamber



Figure 4. 18 New defect characterization system

Before the system could be installed in the lab, several preparations needed to be completed. For example, three phase high voltage plugs are needed for the power supply and a water cooling system is needed for the cooling of the turbo pump.

The inner structure of the defect characterization system is shown in Fig 4.19. At the entrance of the chamber, there are three apertures with different diameters controlled by a motor. Operators can move one of the apertures into the beam line to limit the size of the beam spot. An ion beam is connected to the sample chamber on one side. A temperature controlling system (Hot&Cold Stage) is able to adjust the temperature of the sample from several K to several hundred K. Two high-purity Ge detectors are inserted into the chamber from two sides for coincidence Doppler broadening measurement. The system includes a sample holder and a sample holder plate. Ion implantation and temperature control are only available for the sample on the sample holder. The sample holder plate can support multiple samples. By rotating the sample holder plate, the samples on it can be measured one by one.

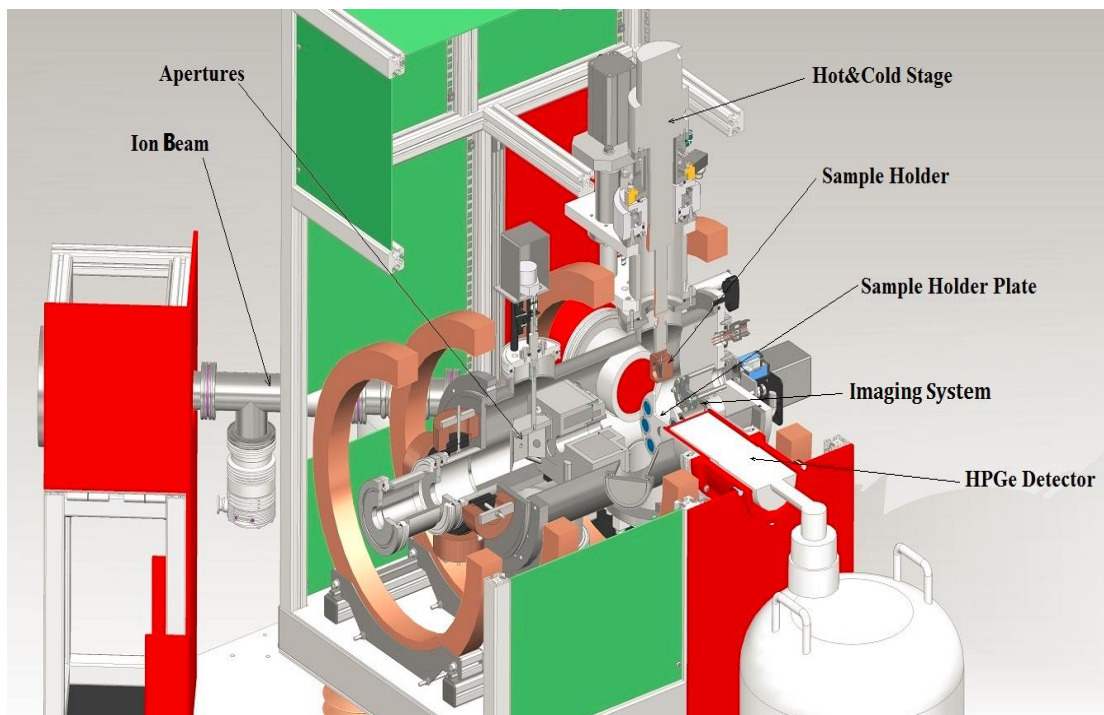


Figure 4. 19 The structures inside the sample chamber^[44]

The system is also equipped with a beam imaging set-up as is shown in Fig. 4.20, which includes three Microchannel Plates (MCP) and a phosphorus screen. A video camera is pointed at the phosphorus screen from the outside that can record in real time the image of the beam on the screen.

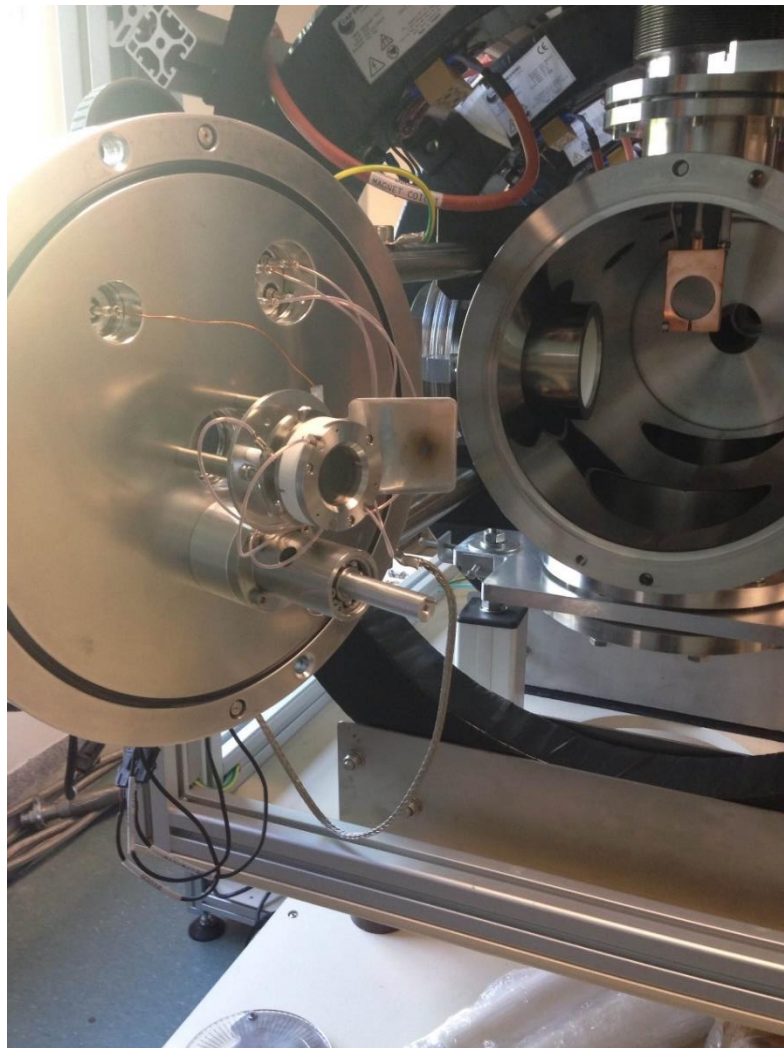


Figure 4. 20 Beam imaging system

4.3.2 Software description

The software used to control the system was designed by CAP Engineering Co. using LabVIEW. Because the system will work under high voltage and high radiation background conditions, almost all of the functions to control the system and the parameters to monitor the processes have been integrated into the software,

so that operators can communicate with the system through Ethernet remote from potential hazards.

The interface of the software is designed to be user-friendly. The tags on the left of the interface can lead to a variety of functions. On the vacuum page (Fig. 4.21), operators can switch the vacuum process between manual and automatic control. The green lights show the status of each part. When a green light is on, it means the corresponding function is working. The readings of two vacuum gauges in the chamber or between the pumps can both be seen in real-time.

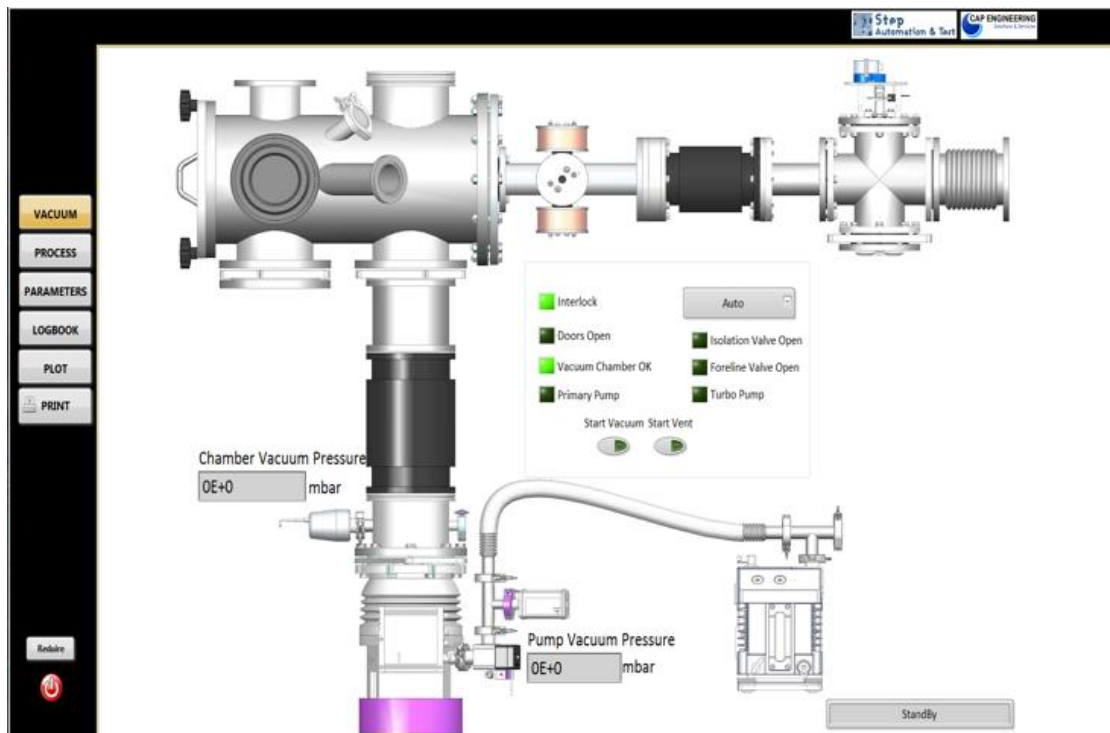


Figure 4. 21 Vacuum control page

On the process page, the main functions of the system can be controlled and monitored in the sub-pages, including Magnets, Process, Motors and Hot&Cold Stage. The Magnets page (Fig. 4.22) includes the current of six main coils and the X-Y steering magnet. On this page, operators also can set the voltage on MCPs and the phosphorus screen. When the imaging system is working, the picture of the screen will show on the right side of the page. The motors page (not shown) includes the controls to adjust the position of sample holders, aperture and detectors.

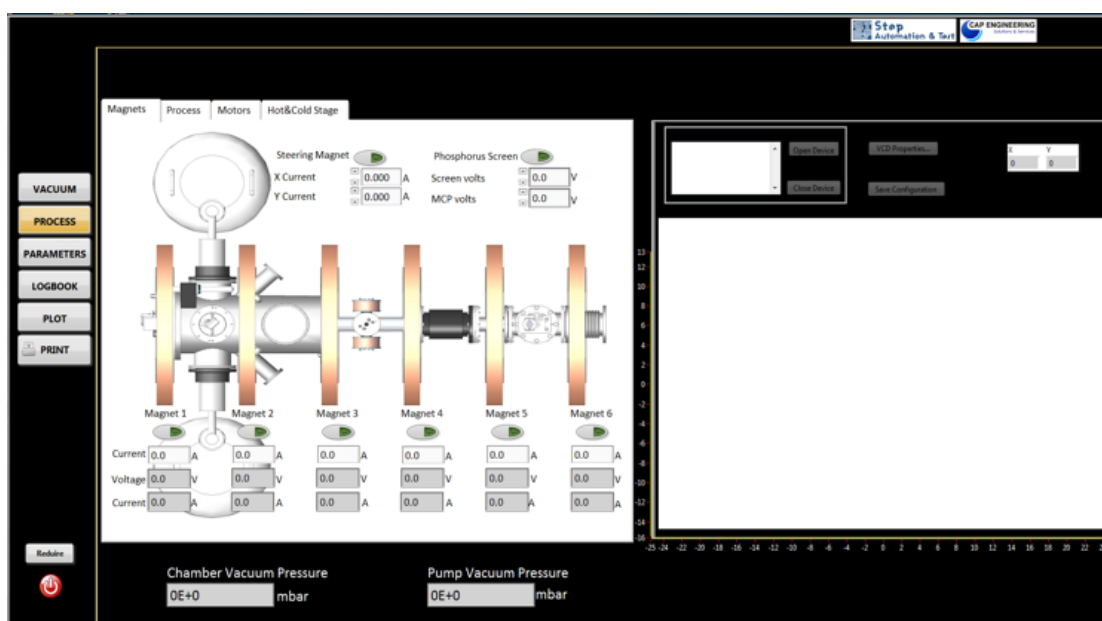


Figure 4. 22 Magnets page

In the Hot & Cold page (not shown), four detectors show the temperatures at different positions in the chamber. Additionally, the settings for ion implantation can be changed in this page, including time duration and current.

On the Plot page (Fig. 4.23), the parameters, such as vacuum and temperature, can be monitored and saved with the change of time. The saved data can be loaded and plotted in a diagram and printed out. In this page, all the settings can be generated in the same page, which makes it easier to check and print.

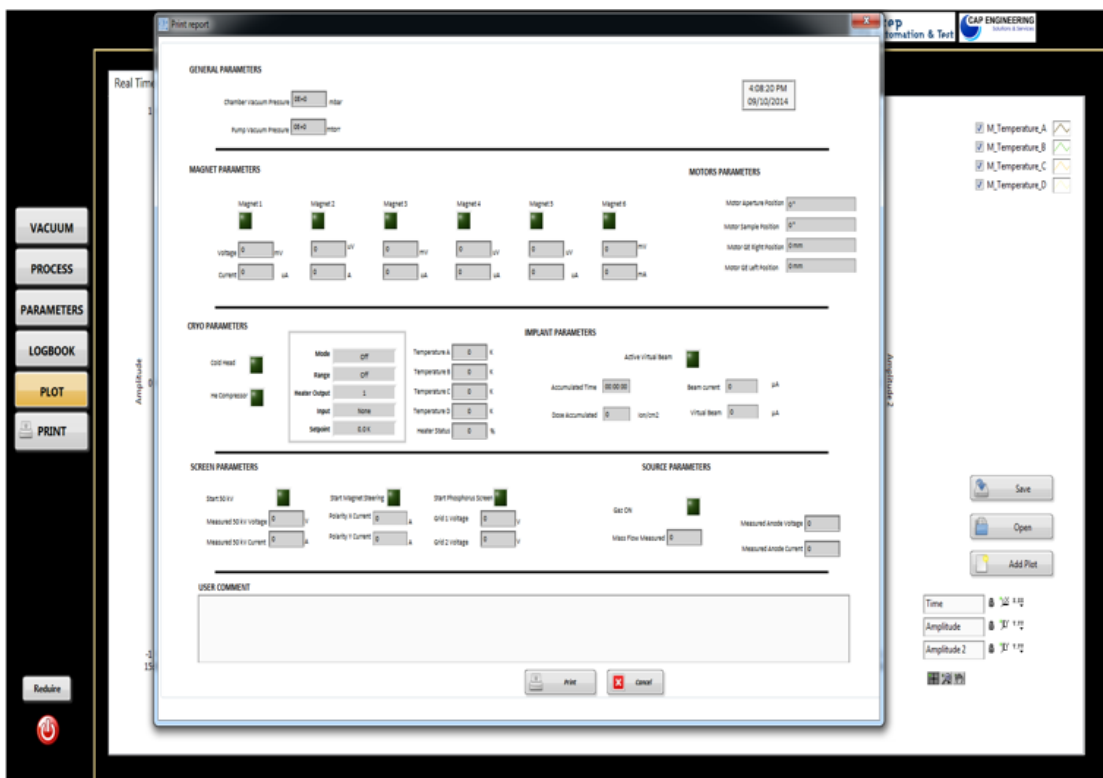


Figure 4. 23 Plot page

4.4 Operation of the system

4.4.1 Vacuum procedure

If the system has not been used for a long time, the vacuum and magnetic field status need to be tested before taking a measurement in order to make sure everything works well. Certain tests need to be done and are listed as follows:

1. Check all the valves. Make sure the valve between the two chambers is closed.
2. Pump down the source chamber:
 - Check the valve between source chamber and turbo pump. Close the valve.
 - Check the valve between turbo pump and roughing pump. Close the valve.
 - Turn on the turbo pump. Leave it running for half an hour. Check the vacuum at the gas inlet with vacuum gauge. It should be less than 200mTorr.
 - Open the two valves between source chamber and roughing pump. Wait until the vacuum of the chamber is below 200mTorr (100mTorr is better).
 - Turn on the turbo pump. Wait until the vacuum of the chamber better than 1mTorr.

- Turn on the ion gauge. Wait until the reading on the ion-gauge is less than 10^{-6} Torr. If the vacuum cannot get better than 10^{-6} Torr, consider checking for leakage.
3. Start the control of sample chamber:
- Push the “Start” button on the main controller to turn on the power
 - Turn on the computer. Wait for several minutes until all software are pre-loaded. Open “Positron” software on desktop.
 - On the vacuum page, the current state of the vacuum chamber is shown. If the vacuum shown on the page is zero, it indicates that communication between the software and the instruments is not connected. Check the connection software to see if all the instruments are connected. If not, try to restart the computer or the controller.
4. Pump down the sample chamber:

Normally, the process is in the standby mode at the beginning. The default control mode is “auto”, which means all steps are pre-set. By clicking the “start vacuum” button, the primary pump will start running. When the vacuum pressure has reached 0.5mbar, the frontline valve will open. When the chamber vacuum has reached 0.1mbar, the turbo pump will start. After the vacuum of the chamber has reached 10^{-5} mbar, the vacuum chamber “OK” light will turn on. The vacuum should

be better than 10^{-6} mbar. Be cautious that the voltage should not be turned on until the vacuum is better than 10^{-6} mbar, or the MCPs will be damaged. When the vacuum between two chambers is better than 10^{-6} mbar, it is time to connect the two chambers by opening the valve between them.

To vent the system, the opposite process of the above should be followed. First, close the valve between the two chambers by clicking off the start vacuum button, followed by clicking on the start vent button. The system will then vent the sample chamber automatically. While the system is currently vented with air, in the future it can be vented with N_2 , which contains less impurities such as water vapor.

4.4.2 Shielding for radiation and high voltage

The highest voltage that can be applied on the sample holder is 50kV. The sample holder is connected to the entire sample chamber. Therefore, when the high voltage is on, the system needs to be well isolated.

To ensure the safety of operators, there is a cage ($2.5 \times 2.5m^2$) surrounding the experimental chamber, as is shown in Fig. 4.24. There are five separate blue keys to lock five doors of the cage. When all the doors are locked, the five keys can be pulled out to unlock a red key outside the cage. The red key can unlock a switch, which will disconnect the cage from the system and ground the cage. At the same

time, a red light will be turned on to alert people to stay away. After that, the high voltage can be turned on.

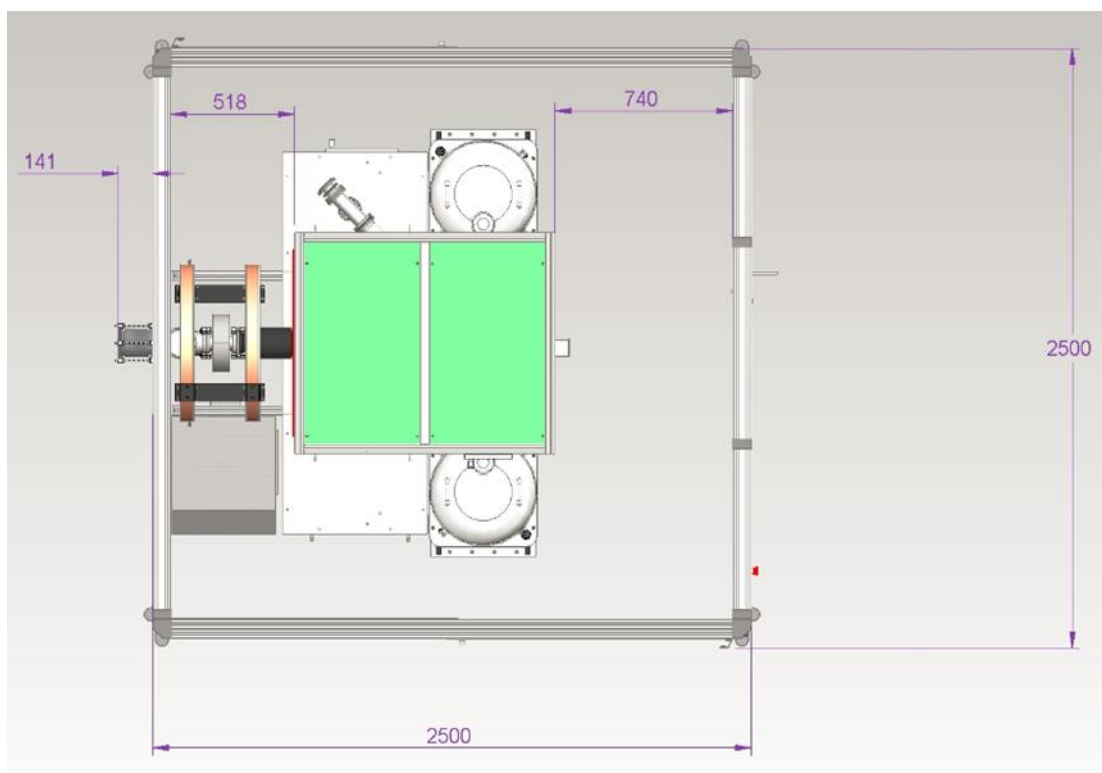


Figure 4. 24 Top view of the defect characterization system in the cage^[44]

(Unit: mm)

While in the cage, attention should be paid to avoid short circuit. Since the spectrum acquisition and analysis system in the cage is directly connected to the computer outside the cage, the spectrum acquisition and analysis system should be insulated from the beam system. The closest distance between the high purity Ge detectors and the chamber is only about 1cm. At the beginning of our test process, a

metal cylinder was inserted at the closest position to simulate the detector. When the high voltage went up to 10 kV, arcing occurred between the cylinder and the chamber. After examination, an interstice between two pieces of insulators was found. The voltage can be increased up to 50kV after applying a layer of insulation glue for about 2mm.

4.4.3 Beam transportation

It is easier to change the setting of the system before installing the source than after. The reason is that once the source is installed, it will not be safe to open the chamber. Therefore, before installation of the positron source, an electron gun as shown in Fig. 4.25 was installed to produce an electron beam to simulate the positron beam. The principle of this test is that the electron has the same mass and amount of charge as the positron does. As for the opposite charge, the only difference is the necessary reversal of the polarity of the accelerating voltage. Another thing to take into consideration is the magnetic field, since the magnetic field is used to focus the positron beam. Based on our calculations, it was found that the magnetic field works as well for electrons as for positrons in the beam transportation. There is no need to reverse the magnetic field.

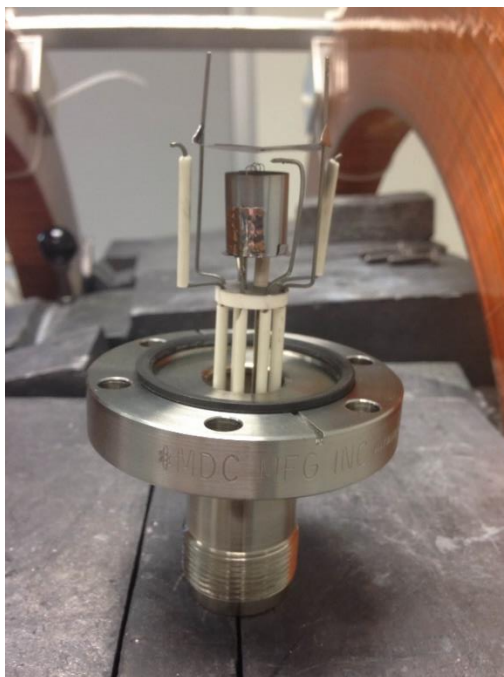


Figure 4. 25 Electron gun

The electron gun was made from a filament with variable voltage applied on it to create electrons. A multi-meter was used to monitor the current through the filament. The current should be lower than 1mA, or the filament will burn through. A wire with a voltage of negative 100V connects to the filament to float it and works as the acceleration voltage. In front of the filament, there is a metal foil with a 1.5mm-diameter small aperture in the center. The foil is insulated from the filament and the size of the aperture is regarded as the size of the electron beam.

It is a long trip (about 3m) for the beam to transport from the source to the target and even a slight change of the magnetic and electric field can direct the beam onto the wall of the chambers. Chances are that the beam could get lost anywhere in the chamber. It is thus necessary to locate the beam in each step of the transportation.

For the electron beam, no moderator is needed. In the following step, the beam will pass through a structure called retarding-field analyzers. There are two same energy analyzers^[45] arranged along the chamber as is shown in Fig. 4.26. Each energy analyzer contains two rectangular copper plates (e.g. P1, P2) and two round copper mirrors (e.g. P3, P4). One of the round mirrors has a hole at the center and the other has a hole on the side. These round mirrors are insulated and grounded. Each pair of the rectangular plates has a voltage applied between them. In the chamber, the area between two rectangular plates will contain an $E \times B$ field when the power is on. The B field is oriented along the axis of the chamber and the E field is directed from one plate to the other. When electrons enter into the field from the hole at the center, the direction will be changed based on the initial speed. Only electrons with specific speeds can pass through the upper hole. In this way, electrons with specific energies are selected. With proper voltage applied on two pairs of the plates, a fraction of the electrons can pass through all four holes.

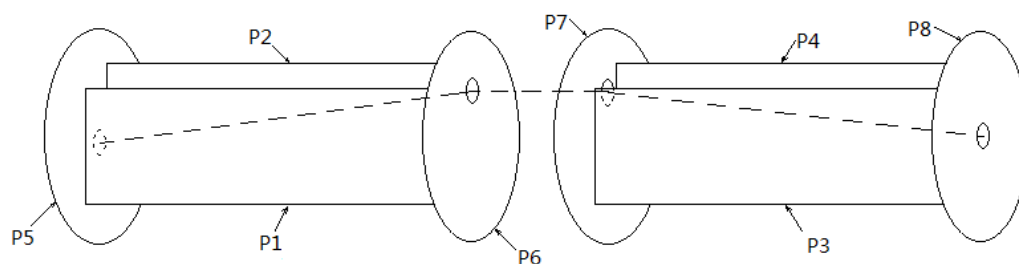


Figure 4. 26 Energy analyzers

It may take a long time for trials to adjust the voltage until most electrons can pass through the various holes. Some settings can be applied to shorten this period, as is shown in Fig. 4.27. To examine whether the beam can pass the first energy analyzer, a copper pin was put between P1 and P2 in the center with a multi-meter connected to it. If electrons pass P7 and P6, there will be current shown on the meter. The voltage between P3 and P4 was continuously being adjusted until the maximum current arrives on the pin. Upon this time, most of the electrons with selected energies can pass through the first energy analyzer. A removable Aluminum plate was placed behind P5 with a hole in the center, behind which an Aluminum foil was placed. The Al plate, the Al foil and the chamber are insulated. The foil should be larger than the hole in the plate and smaller than the plate. The voltage between P1 and P2 was continuously being adjusted until the maximum current occurred on the Al foil and minimum current occurred on the Al plate. For now, the majority of the electrons can pass through the energy analyzers.

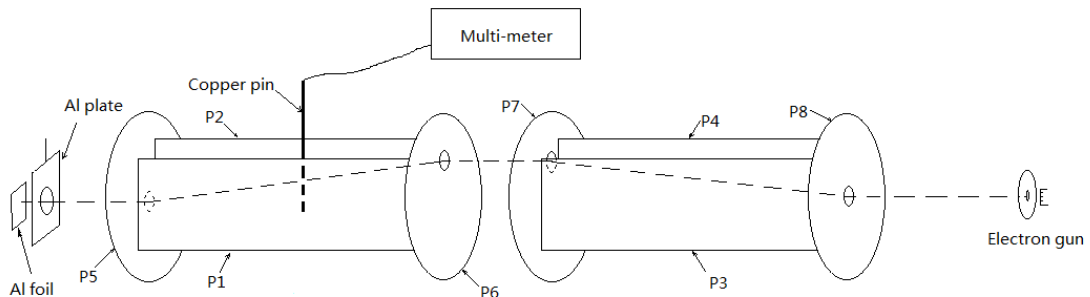


Figure 4. 27 Beam transportation

The beam profile was monitored by a micro-channel plate (MCP) detector with a phosphorus screen and a CCD-camera which was fixed on the end of the beam line. The copper pin, Al plate and Al foil used in the previous step can be removed. After turning on the imaging system, a voltage can be applied on the MCPs and the phosphorus screen. Based on the operating manual of the imaging system, the maximum voltage between two MCPs is 1000V, while the maximum voltage between MCP and phosphorus screen is 4000V. The next step is to adjust the magnetic field of the source chamber to focus the beam on the MCPs until the beam spot is bright enough on the phosphorus screen. During this procedure, a shape looking like the “milky way” may appear on the screen as shown in Fig. 4.28 (1). However, this is not the real beam spot. To identify if the shape is the beam spot, a temporary setting was used on the sample holder, as is shown in Fig. 4.29. An insulated aluminum foil was used to cover the position of sample. A multi-meter was used to measure the current on it. When the “milky way” was shown on the screen, there was almost no current on the film. That means the signal came from the reflection off the wall of the chamber and one needs to adjust the X-Y magnetic field to get the maximum current on the foil. After moving away the sample holder, the beam spot will show on the screen as shown in Fig. 4.28(2).

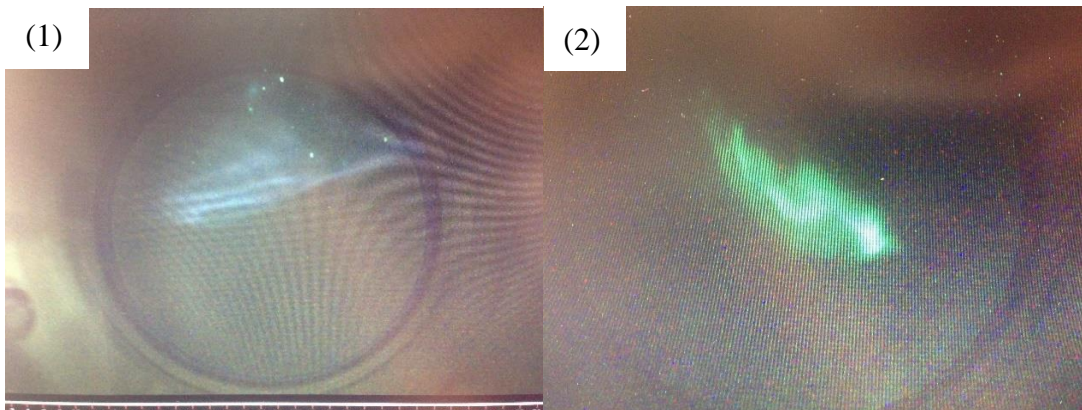


Figure 4. 28 Shape on the screen (1) “milky way” (2) real beam spot



Figure 4. 29 Aluminum film on the sample holder to collect the beam current

4.4.4 Moderator preparation and installation

In this system, a tungsten film is used as the moderator. The single crystal tungsten foil is about 1 μm thick. Since the original tungsten contains defects (for example, vacancies) that may trap positrons, it needs to be annealed in a separate vacuum chamber at a temperature around 2500°C^[46]. During the annealing, a certain amount of carbon may precipitate to the surface^[46]. Some oxygen thus needs to be released into the chamber to burn off the carbon.

The tungsten foil is placed on a ring with a diameter of about 1cm as shown in Fig 4.30. It will be delivered into the chamber and placed right in front of the source supported by a stick. Since the metal of the ring is very soft, care needs to be taken when putting the source into the chamber. Once it touches the wall, it will be bent and the tungsten foil may break. The small windows on the chamber will be helpful. The procedure to change the moderator should be implemented before the source installation in order to make sure the moderator is placed in the right position.

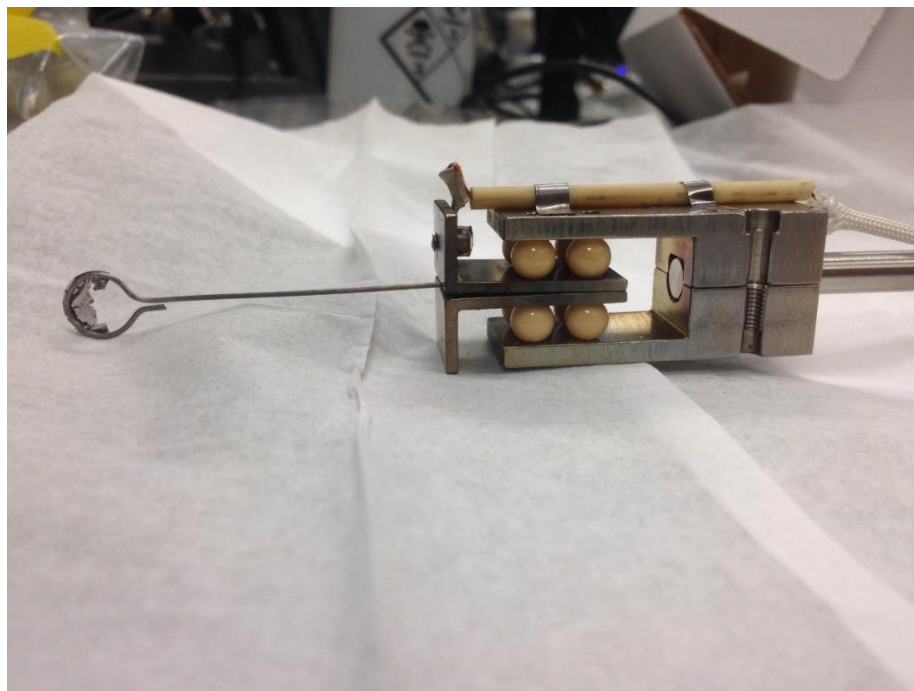


Figure 4. 30 Moderator assembly (the moderator foil in the picture is broken)

4.4.5 Source installation

The new positron source used in the lab is solid ^{22}Na compound purchased from the iThemba Laboratory for Accelerator Based Sciences (LABS) in South Africa. It was delivered in a lead can as shown in Fig. 4.31. The activity of the source is: 1110MBq (30mCi) on 12 June 2014.

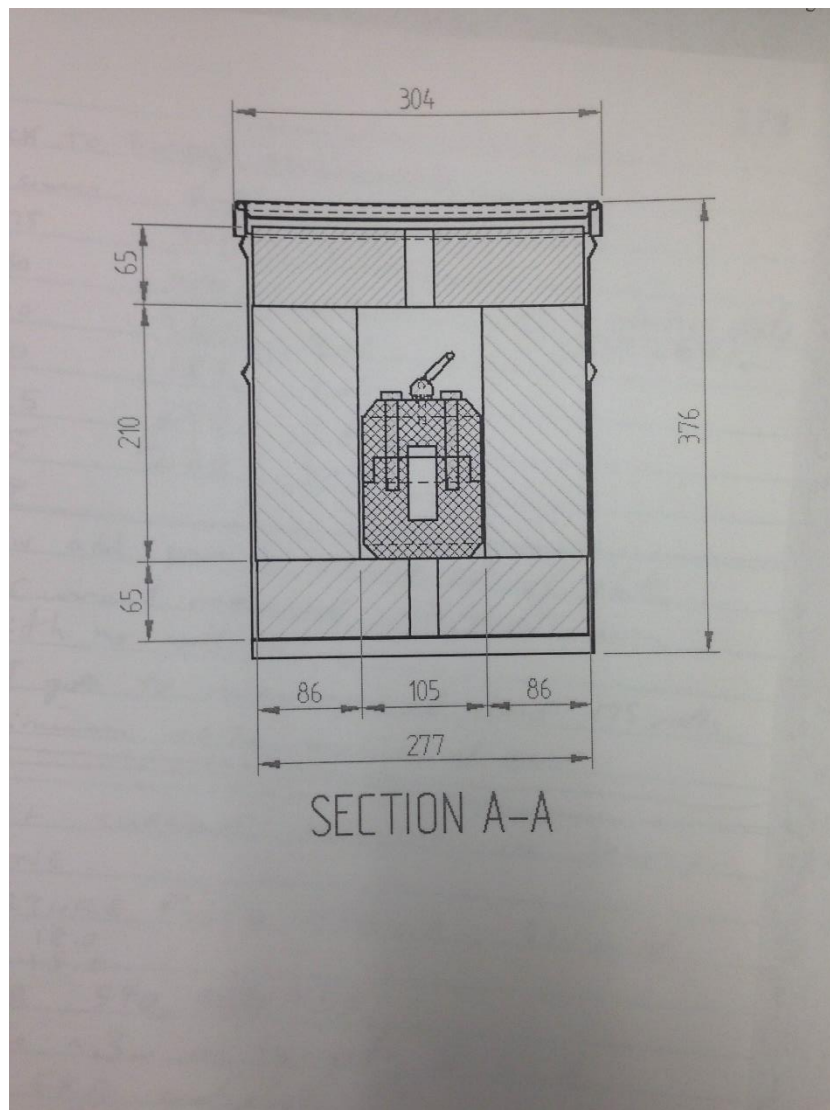


Figure 4. 31 Schematic of the source container

The activity of the source is very high. Therefore, everything should be ready before trying to open the shielding and transporting the source.

- Put enough shielding around the source chamber, and leave some additional lead blocks by the side.

- Become familiar with the structure of the source holder from the drawing
- Find the right screw driver for the source holder: 7/64 inch
- Prepare at least one cart to transport the source and shielding
- Prepare one source container and a pair of tweezers
- Based on the position to operate, place enough shielding on the cart, including one specifically made to temporarily contain the source
- Wear an electronic dosimeter, gloves, and put a radiation detector by the side during the entire procedure. Try to keep most of the body behind the shielding and stay the least amount of time.
- Open the shielding of the old source, take out the source holder. Use screw driver to dismount the source into the source container.
- Place some paper in front of the temporary holder to adjust the height and make sure the source holder can go directly into the container
- Open the shielding of the new source, use tweezers to place it on the source holder then fasten the screw.
- Quickly move the source into the temporary holder on the cart. Then move the cart close to the source chamber.
- Quickly move the source holder into the chamber. Then shield the chamber with lead blocks.

- Use radiation detector to measure everything that source contacted, make sure no radiation material is left and no contamination has occurred. The reading should be about 0.2-0.4uSv/h. Any part outside the chamber should not exceed 2.5uSv/h.

The total amount of radiation exposure during one-time operation for an operator is about 3uSv.

4.4.6 Search for the positron beam

After switching from the electron to the positron beam, the first thing that needs to be considered is if it is necessary to change the direction of the electromagnetic field in order to transport the positrons. The voltage to accelerate positrons needs to be positive. The positive voltage on the source is optional, because the energy distribution of the positrons emitted from the ^{22}Na source is from 0 to 545keV. Compared with the initial energy of the positrons, the hundreds of volts acceleration voltage will not make much of a difference. The positive voltage to accelerate the positrons is applied to the tungsten moderator because the moderated positrons emitted from the surface have energies of only a few eV. This acceleration voltage is normally selected between 100 and 200V. This voltage is only used to transport the moderated positrons to the sample chamber. The variable

high voltage for the positron implantation will be directly applied to the sample. There is a grid parallel to the moderator behind it to form a uniform electric field between them to guide the positrons. The voltage on the grid can be a fixed value between 0 and the voltage on the moderator.

Classically, the Lorentz force can be calculated from the formula below:

$$\mathbf{F} = q(\mathbf{V} \times \mathbf{B}) \quad (4.1)$$

In equation (4.1), q is the charge of the particle, $-e$ for the electron and $+e$ for the positron; \mathbf{V} is the velocity of particle and \mathbf{B} is the magnetic field. In magnetic field, when the electron is replaced by the positron, q will change from $-e$ to $+e$. That is to say positrons will move forward in a helical motion with an opposite direction to that of electrons. It will not affect the size of the beam. In the electromagnetic field between energy analyzers, however, the action of the Lorentz force can also change the direction of the beam to go through the holes. The directions of accelerations for the positrons and the electrons in the electric field are opposite and they have opposite charges. In combination, the additional Lorentz force applied to the positron and the electron is in the same direction. As the result, the direction of the electromagnetic field will not need to be changed. In the previous setting, the surface of the first MCP is grounded because the electron beam is rather intense. Now for positrons, a negative voltage of 100V is applied to the surface of the first

MCP to attract the beam. The other voltages on the MCPs and phosphor screen will not need to be changed.

Besides the changes discussed above, the same setting as the electron beam was used. The positron beam is supposed to arrive at MCPs in this setting.

The intensity of the moderated positron beam is far below that of the electron beam (the current of the positron beam is at the fA level and the current of the electron beam is at the μA level). Therefore, it is impossible to use an ammeter to find the positron beams as we used to find the electron beam. The property of positron annihilation can be utilized at this time. A scintillator detection system as shown in Fig. 4.32 can be used to detect the 511keV gamma rays. A pre-amplifier is included in the detector. A positive $\sim 1000\text{V}$ high voltage is applied to the detector and a 12-24V voltage is applied to the pre-amplifier. Before applying this detector to find the beam around the chamber, some settings need to be done. The scale on the discriminator of single channel analyzer (SCA) needs to be appropriate for the energy. The first method discussed in section 4.3.1 is applied to find the 511keV energy peak on the discriminator. A $1\mu\text{Ci } ^{22}\text{Na}$ source was put in front of the detector. The upper level and lower level are adjusted on the SCA to limit the energy range to around 511keV. Then, the detector is moved to several positions of the chamber and the rate of γ rays is determined. Also, the detector can be fixed at a certain position and the voltage settings of the beam can be changed. By counting

for a period of time, the change of count rate can be compared. When measuring the count rate, the radiation from the source part needs to be shielded. The reason is that the moderation efficiency is relatively low and thus, the change of the count rate may not be significant compared with the background.

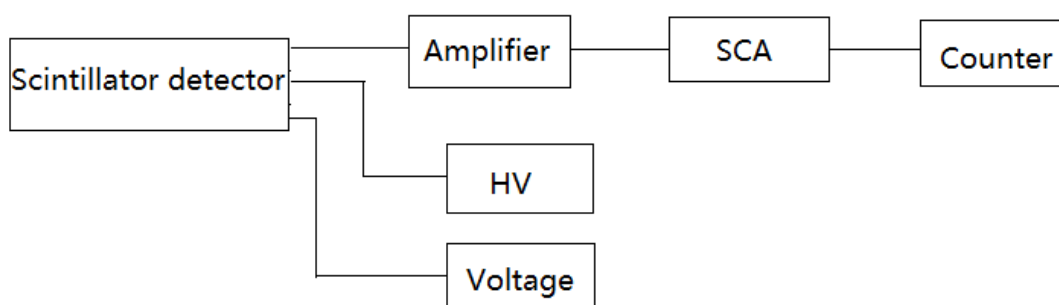


Figure 4. 32 Schematic of scintillator detector electronics

In this method, every time a parameter is changing, a period of time such as 100s needs to be counted for several times. There is, however, a faster way to observe the change of count rate: connect a rate meter and a rate monitor following the SCA as shown in fig. 4.33.

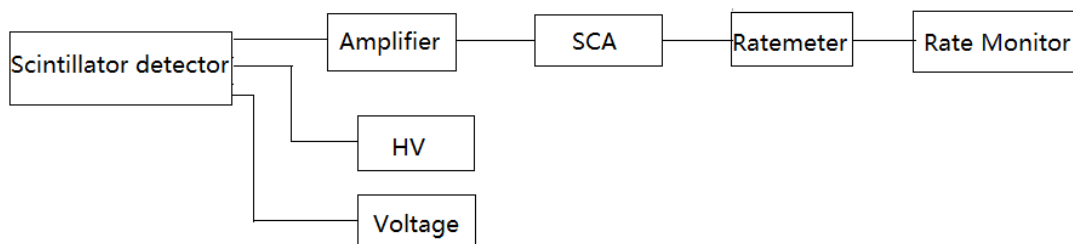


Figure 4. 33 Modified schematic for scintillator detector electronics

The rate meter is used to convert the count rate to a voltage between 0 and 10V. The rate monitor is used to convert the voltage signal to sound of noise with specific frequency. When the count rate changes, the change of noise frequency can be distinguished by ear. When moving the detector from one place to another, the change of radiation count rate can be recognized in real time.

4.4.7 Ion beam and temperature control

The compressor for temperature control is not connected to the software at present because the power for the controller is not enough. When adjusting the temperature, the first step is to turn on the compressor: click on Cold Head in the controlling software and the temperature will start to decrease. After about 45 minutes, the temperature at the cold head can reach around 7K and the temperature at the sample holder is several degrees higher.

There are four temperature sensors (A, B, C and D) in the sample chamber. A is on the cold head and B, C, and D are near the sample. The sensor A (a silicon

diode) is mainly used to monitor the temperature of the cold head to keep the cold head working in a normal temperature (below 325K). The sensor B (platinum sensor) is the most accurate one in a large temperature range from 77K to 1000K and it is mainly used for calibration. The sensor C (gold sensor) is calibrated for the low end (~4K) and it will stop working when the temperature goes above 610K. The sensor D is a K-type thermocouple and it is specially calibrated to accurately read the temperature at 1000K. In this way, the temperature from several to several hundred K can be monitored. When heating or cooling the sample, the cold head should always be active to keep the temperature stable.

The ion beam is installed on one side of the sample chamber, as is shown in Fig. 4.34. When operators set the sample holder to the implantation position in the controlling software, the ion gun can directly point at the sample on the sample holder. To use the ion implantation modality, the gas for ion source needs to be connected to the ion gun. The pressure of the gas should be between 1~2atm. Some parameters need to be obtained before starting the implantation. A convenient way to know the size of the ion beam is to put a piece of paper to cover the sample holder. After turning on the ion beam, the ion beam will burn the paper with a spot. By measuring the size of the spot, the size of the ion beam can be calculated and input in the software.

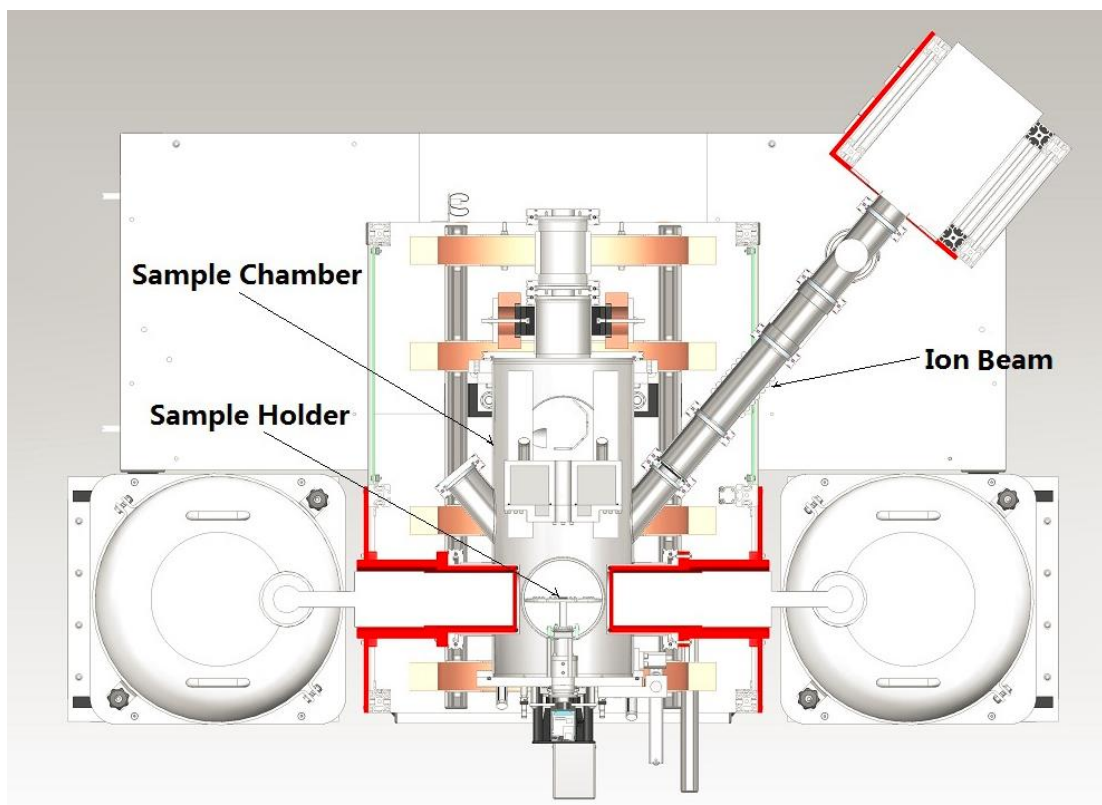


Figure 4. 34 Top view of the ion beam connected to the sample chamber^[44]

When the sample holder is in the Up position, the ion gun is directly pointing to a metal plate behind the sample holder. It is the time to turn on the ion beam and voltage to get the current on the plate. When the desired stable current arrives, operators can type it in the virtual current and input total dose for the implantation in the software. Then operators can start the implantation by setting the sample holder to the implantation position and clicking the start button. When the required dose is reached, the implantation will stop automatically. The maximum anode current is

13mA and the maximum implantation voltage is 6000V. The measured value is a balance of these two.

Chapter 5 - Summary and Prospects

5.1 Summary

In this thesis, the development of intense beam facilities in the world has been reviewed and the progress in installing MIPBF has been described in detail. The spectrum acquisition and analysis system was tested and adjusted. A brief coincidence CDBS system has been set up, which is ready to do measurement. The new defect characterization system has been connected with the source chamber. The installation procedure and operation steps are listed. The system has been successfully tested with an electron beam.

5.2 Future work

Many improvements are planned to be realized in near future. The next step is to locate the positron beam. Based on the position of the beam spot on phosphorus screen, the magnetic field and the electric field at each part of the system can be adjusted to focus the beam on the center of the screen. By recording the optimized setting of the magnetic field and the electric field at each acceleration voltage, a database can be established. After that, testing experiment can be operated manually at different positron energies.

In order to collect data more efficiently, the system could run automatically. A program could be coded with all the system settings at each acceleration voltage. It would thus be able to control the magnetic and the electric fields, and change the value of them at the same time with the changing of the acceleration voltage. Then the program can be combined with the Mestro software to loop the experiment and collect data automatically.

During the process to optimize the system, some standard samples can be measured and the results can be used to compare with those in published papers. When the installation and adjustment of the positron source part in the MNR is finished, the defect characterization system can be transported to McMaster University and installed in the reactor. After connection with the intense source, more meaningful experiments will be launched and exciting data can be expected.

Bibliography

- [1] Dirac, Paul AM. "Quantised singularities in the electromagnetic field." Proceedings of the Royal Society of London A: Mathematical, Physical and Engineering Sciences. Vol. 133. No. 821. The Royal Society, 1931.
- [2] Anderson, Carl D. "The apparent existence of easily deflectable positives." *Science* 76 (1932): 238-239.
- [3] Dirac, P. A. M. "On the annihilation of electrons and protons." *Mathematical Proceedings of the Cambridge Philosophical Society*. Vol. 26. No. 03. Cambridge University Press, 1930.
- [4] Schultz, Peter J., and Kelvin G. Lynn. "Interaction of positron beams with surfaces, thin films, and interfaces." *Reviews of Modern Physics* 60.3 (1988): 701.
- [5] Manual of PLS-System from Ortec
- [6] Mogensen, Ole Erik. *Positron annihilation in chemistry*. Springer, 1995.
- [7] Lynn, K. G., and A. N. Goland. "Observation of high momentum tails of positron-annihilation lineshapes." *Solid State Communications* 18.11 (1976): 1549-1552.
- [8] MacDonald, Jack R., et al. "A two-dimensional Doppler broadened technique in positron annihilation." *Nuclear Instruments and Methods* 153.1 (1978): 189-194.
- [9] Wang, Shaojie, et al. *Applied Positron Spectroscopy*. Hubei Science and Technique, 2008.
- [10] L. Madanski and F. Rasetti, *Phys. Rev.* 79,397(1950)
- [11] Schultz, Peter J., and Kelvin G. Lynn. "Interaction of positron beams with surfaces, thin films, and interfaces." *Reviews of Modern Physics* 60.3 (1988): 701.
- [12] Hugenschmidt, C., B. Straßer, and K. Schreckenbach. "Investigation of positron work function and moderation efficiency of Ni, Ta, Pt and W (1 0 0)." *Applied surface science* 194.1 (2002): 283-286.
- [13] Greaves, R. G., and C. M. Surko. "Solid neon moderator for positron-trapping experiments." *Canadian Journal of Physics* 74.7-8 (1996): 445-448.

- [14] Surko, Clifford M., M. Leventhal, and A. Passner. "Positron plasma in the laboratory." *Physical Review Letters* 62.8 (1989): 901.
- [15] Greaves, R. G., M. D. Tinkle, and C. M. Surko. "Creation and uses of positron plasmas*." *Physics of Plasmas* (1994-present) 1.5 (1994): 1439-1446.
- [16] Gilbert, S. J., et al. "Creation of a monoenergetic pulsed positron beam." *Applied Physics Letters* 70.15 (1997): 1944-1946.
- [17] AIST: https://unit.aist.go.jp/riif/posiprobe/facilities/linac_en.html
- [18] Oshima, Nagayasu, et al. "Development of positron microbeam in AIST." *Materials Science Forum*. Vol. 607. 2009.
- [19] Oshima, Nagayasu, et al. "Brightness enhancement method for a high-intensity positron beam produced by an electron accelerator." *Journal of Applied Physics* 103.9 (2008): 094916.
- [20] Oshima, N., et al. "Rapid three-dimensional imaging of defect distributions using a high-intensity positron microbeam." *Applied Physics Letters* 94.19 (2009): 194104.
- [21] Wang, Bao Yi, et al. "The slow positron beam based on Beijing electron-positron collider." *Materials Science Forum*. Vol. 445. 2004.
- [22] Cao, Xing-Zhong, et al. "Performance of Beijing intense slow positron beam." *High Energy Physics and Nuclear Physics* Vol. 30. No. 12. (2006).
- [23] Jonah, Charles D., et al. "Development of the Argonne positron source APosS." *Applied Surface Science* 255.1 (2008): 25-28.
- [24] Chemerisov, Sergey, and Charles D. Jonah. "Development of high intensity source of thermal positrons APosS (Argonne Positron Source)." *Journal of Physics: Conference Series*. Vol. 262. No. 1. IOP Publishing, 2011.
- [25] Krause-Rehberg, R., et al. "EPOS—An intense positron beam project at the ELBE radiation source in Rossendorf." *Applied surface science* 252.9 (2006): 3106-3110.
- [26] Krause-Rehberg, R., et al. "Use of superconducting linacs for positron generation: the EPOS system at the Forschungszentrum Dresden-Rossendorf (FZD)." *Journal of Physics: Conference Series*. Vol. 262. No. 1. IOP Publishing, 2011.

[27] Rey, J. M., et al. "Status of the Linac based positron source at Saclay." *Journal of Physics: Conference Series*. Vol. 443. No. 1. IOP Publishing, 2013.

[28] Liskay, L., et al. "Present status of the low energy linac-based slow positron beam and positronium spectrometer in Saclay." *Journal of Physics: Conference Series*. Vol. 505. No. 1. IOP Publishing, 2014.

[29] Hugenschmidt, C., et al. "Intense positron source at the Munich research reactor FRM-II." *Materials Science Forum*. Vol. 363. 2001.

[30] Davies, Handel, H. A. Bethe, and L. C. Maximon. "Theory of bremsstrahlung and pair production. II. Integral cross section for pair production." *Physical review* 93.4 (1954): 788.

[31] Van Veen, A., et al. "The design of a nuclear - reactor - based positron beam for materials analysis." *The fifth international workshop on slow positron beam techniques for solids and surfaces*. Vol. 303. No. 1. AIP Publishing, 1994.

[32] Van Veen, A., et al. "Positron extraction and transport in a nuclear-reactor-based positron beam." *Nuclear Instruments and Methods in Physics Research Section A: Accelerators, Spectroscopy, Detectors and Associated Equipment* 427.1 (1999): 266-270.

[33] Van Veen, A., et al. "Intense positron sources and their applications." *Materials Science Forum*. Vol. 363. 2001.

[34] Schut, H., et al. "Long term performance of the reactor based positron beam POSH." *Materials Science Forum*. Vol. 445. 2004.

[35] Hugenschmidt, C., et al. "First positron experiments at NEPOMUC." *Applied surface science* 252.9 (2006): 3098-3105.

[36] Hugenschmidt, C., et al. "First platinum moderated positron beam based on neutron capture." *Nuclear Instruments and Methods in Physics Research Section B: Beam Interactions with Materials and Atoms* 198.3 (2002): 220-229.

[37] Hugenschmidt, Christoph, et al. "The NEPOMUC upgrade and advanced positron beam experiments." *New Journal of Physics* 14.5 (2012): 055027.

[38] Hugenschmidt, C., et al. "Positron Beam Characteristics at NEPOMUC Upgrade." *Journal of Physics: Conference Series*. Vol. 505. No. 1. IOP Publishing, 2014.

- [39] Hawari, Ayman I., et al. "The intense slow positron beam facility at the NC state university PULSTAR reactor." *APPLICATION OF ACCELERATORS IN RESEARCH AND INDUSTRY: Twentieth International Conference*. Vol. 1099. No. 1. AIP Publishing, 2009.
- [40] Hawari, Ayman I., et al. "Operation and testing of the PULSTAR reactor intense slow positron beam and PALS spectroscopy." *Journal of Physics: Conference Series*. Vol. 262. No. 1. IOP Publishing, 2011.
- [41] Zeman, A., et al. "High intensity positron source at HFR: Basic concept, scoring and design optimisation." *Nuclear Instruments and Methods in Physics Research Section B: Beam Interactions with Materials and Atoms* 271 (2012): 19-26.
- [42] Sato, K., et al. "Development of a mono-energetic positron beam line at the Kyoto University Research Reactor." *Nuclear Instruments and Methods in Physics Research Section B: Beam Interactions with Materials and Atoms* 342 (2015): 104-107.
- [43] Day, S. E. "Positron source design analysis for the McMaster nuclear reactor." (2010).
- [44] Provided by Pierre CARIÉS, Cap Engineering company in France.
- [45] Schultz, Peter J., and Kelvin G. Lynn. "Interaction of positron beams with surfaces, thin films, and interfaces." *Reviews of Modern Physics* 60.3 (1988): 701.
- [46] Vehanen, A., et al. "Improved slow-positron yield using a single crystal tungsten moderator." *Applied Physics A* 32.3 (1983): 163-167.

Appendix A

Table A. 1 Count rate with the change of the scale on discriminator

Lower Limit	#1	#2	#3	Average		An+1-An	Uncertainty
5	196	169	208	191		191	16
4.9	223	211	206	213	191	22	7
4.8	241	257	225	241	213	28	13
4.7	264	230	273	256	241	15	19
4.6	261	299	270	277	256	21	16
4.5	312	318	302	311	277	34	7
4.4	328	335	356	340	311	29	12
4.3	397	419	406	407	340	68	9
4.2	460	513	455	476	407	69	26
4.1	537	541	579	552	476	76	19
4	546	584	563	564	552	12	16
3.9	618	589	608	605	564	41	12
3.8	621	657	670	649	605	44	21
3.7	668	669	669	669	649	19	0
3.6	738	714	703	718	669	50	15

3.5	781	773	726	760	718	42	24
3.4	775	792	793	787	760	27	8
3.3	853	796	831	827	787	40	23
3.2	907	922	934	921	827	94	11
3.1	938	979	923	947	921	26	24
3	1037	969	1013	1006	947	60	28
2.9	998	973	1037	1003	1006	-4	26
2.8	1075	1075	1116	1089	1003	86	19
2.7	1119	1100	1093	1104	1089	15	11
2.6	1130	1213	1144	1162	1104	58	36
2.5	1210	1207	1192	1203	1162	41	8
2.4	1277	1223	1319	1273	1203	70	39
2.3	1269	1366	1309	1315	1273	42	40
2.2	1356	1375	1367	1366	1315	51	8
2.1	1418	1425	1475	1439	1366	73	25
2	1542	1511	1555	1536	1439	97	18
1.9	1636	1566	1617	1606	1536	70	30
1.8	1761	1818	1780	1786	1606	180	24
1.7	1922	1949	1976	1949	1786	163	22

1.6	2303	2282	2220	2268	1949	319	35
1.5	2353	2377	2343	2358	2268	89	14
1.4	2399	2379	2363	2380	2358	23	15
1.3	2495	2500	2457	2484	2380	104	19
1.2	2538	2557	2642	2579	2484	95	45
1.1	2589	2639	2639	2622	2579	43	24
1	2721	2757	2694	2724	2622	102	26
0.9	2749	2729	2884	2787	2724	63	69
0.8	2875	2804	2895	2858	2787	71	39
0.7	2850	2839	2803	2831	2858	-27	20
0.6	2943	2905	2968	2939	2831	108	26
0.5	2974	2959	2919	2951	2939	12	23
0.4	2953	2900	2905	2919	2951	-31	24
0.3	2841	2870	2861	2857	2919	-62	12
0.2	2750	2738	2664	2717	2857	-140	38
0.1	7708	7037	7085	7277	2717	4559	306
					7277		